2019

Modeling and Analyzing a Patch of Human Red Blood Cell by Coarse-Grained Particle Method

Orhan Kaya
Lehigh University, orhankaya.us@gmail.com

Modeling and Analyzing a Patch of Human Red Blood Cell by Coarse-Grained Particle Method

by Orhan Kaya

A Thesis

Presented to the Graduate and Research Committee

of Lehigh University

in Candidacy for the Degree of

Master of Science

in

Department of Mechanical Engineering and Mechanics

Lehigh University

Jan - 2019

Thesis is accepted and approved in partial fulfillment of the requirements for the Master of Science in Department of Mechanical Engineering and Mechanics.

Date Approved

Dr. Yaling Liu, Thesis Advisor

Dr. Gary Harlow,

Chairperson of Department of Mechanical Engineering and Mechanics

ACKNOWLEDGMENTS

First and foremost, I would like to dedicate this thesis to my family, including my mother Yazgül Kaya, my sister, Duygu Kaya, and my father, Hıdır Kaya. As someone who was not able to go to school, my mother dedicated her life to me. She invested all her time and energy, in working nonstop to finance my education.

Second, I would like to thank my advisor, Dr. Yaling Liu, who gave me the opportunity to pursue my Master of Science at his excellent interdisciplinary research laboratory and to purchase a mini workstation to run my simulation on it. His laboratory allowed me to acquire high-quality knowledge and taught me how to do real research not only in my research area but also in diverse research fields with different scopes. His laboratory gave me the first substantial step into the world of research.

Third, I would like to express my sincere appreciation to the Ministry of National Education, the Republic of Turkey, for its financial support through my master education.

Next, thanks go to Doruk Erdem Yunus for the collaboration on Short Fiber Reinforced 3D Printed Ceramic Composite with Shear-Induced Alignment project. In addition to that, I would like to express my gratitude to Meghdad Razizadeh and Ratul Paul for collaboration on LAMMPS and Red Blood Cell damage analysis projects. I would like to extend my thanks to all present and previous Bio Nano Mechanics Lab's valuable members for collaboration on the numerous exciting research projects at the Sinclair Lab, and thanks to good friends and faculty members over fifty at Lehigh University for discussions on scientific topics.

TABLE OF CONTENTS

CHAPTER II

CGMD MODEL FOR A PATCH OF A HUMAN RED BLOOD CELL

CHAPTER III

RESULTS, CONCLUSION AND FUTURE WORK

LIST OF FIGURES

LIST OF TABLES

Abstract

This thesis consists of three sections. First, some background information and theories about the erythrocyte membrane are provided. Second, a coarse-grained molecular dynamics model for a patch of erythrocyte membrane is built up. Third, the mechanical responses of the patch of red blood cells to diffusion and diffusivity, tension, rupture, and shear-induced pore area are analyzed.

The patch of erythrocyte membrane is validated by modeling diffusivity and determining the diffusion coefficient constant. Then, the patch of the coarse-grained erythrocyte membrane is stretched uniformly until rupture. The critical stress/strain from simulation match with those obtained in experiments in laser optical tweezers trapping a bead. Lastly, the pore area of the patch of erythrocyte membrane at the high-stress region is determined over a range of deformations.

The purpose of creating the patch of erythrocyte membrane is to reduce computational cost, obtain accurate and detailed answers from our interested regime conditions, and transfer some quantities from nanoscale to mesoscale by solving time and length scale gaps.

Chapter I. INTRODUCTION

1.1 – Red Blood Cell

Human red blood cells (erythrocytes) primarily transport oxygen from the lungs to body tissues and carbon dioxide from the tissues to the lungs through the circulatory system. Their shape is oval biconcave, and their diameter is between 6.2 and 8.2 micrometers. The thickness in the center is about 0.8-1 micrometers, and at the edge, it is about 2-2.5 micrometers [1]. Erythrocyte volume distribution illustrates statistically and graphically that the average volume of a single RBC cell is about 90 fL with a surface area of 136 μm^2 [2]. The total number of erythrocytes in the human body is roughly 20-30 trillion at any moment, and their rate is 70%, including whole cells [3]. In addition, they are so flexible that their structure allows to squeeze through channels that are narrower than their size, as well.

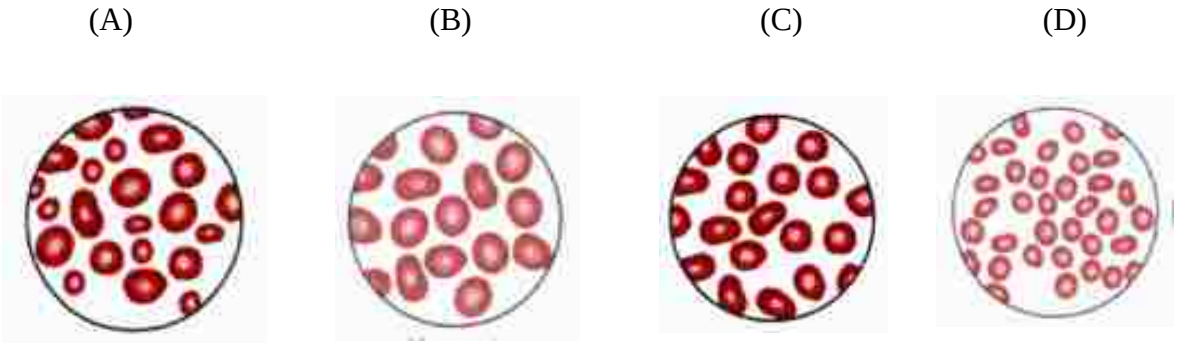

Figure 1.1 Classification of human red blood cells: (a) RBCs that are unequal in size are referred to as anisocytosis. (b) Macrocytic anemia is a condition in which RBCs are more extensive than their average volume. (c) RBCs with their average volume. (d) Microcytic is a condition that RBCs are smaller than their average volume [1].

Having presented some geometrical features along with the classification of human red blood cells, the RBCs' route through the circulatory system can now be described. In the process of red blood cells circulate through the body, they pass through three types of blood vessels that are classified as arteries, veins, and capillaries. Arteries transport blood away from the heart, veins transport them toward the heart and capillaries are connecting branch between the arterioles and venules [4].

(A) (B)

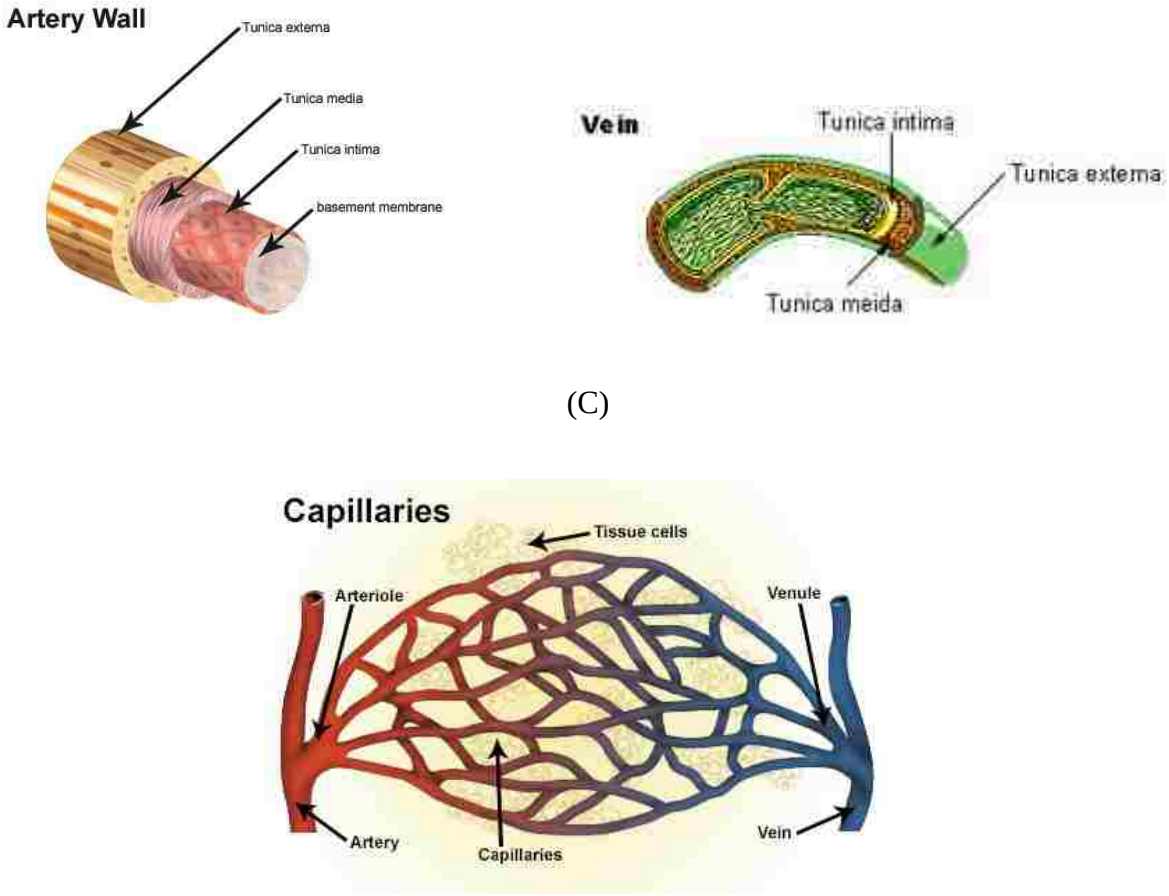

Figure 1.2 Types of blood vessels (a) Artery wall consists of three layers surrounded by a basement membrane. (b) Tube-formed vessels, transport oxygen-depleted blood. (c) Capillaries are connecting branches between the arterioles and venules [4].

Capillaries are the smallest vessels and just big enough for red blood cells to pass through them in a single line. RBCs become deformed while traveling through capillaries because, at the starting and stopping points of capillaries, RBCs can rapidly change their shapes results in an acceleration of flow. Capillary diameters range from 3 micrometers to 10 micrometers. Within these diameters, some take up different shape configurations such as parachute or umbrella, while others take the form of rolls [5].

(A)

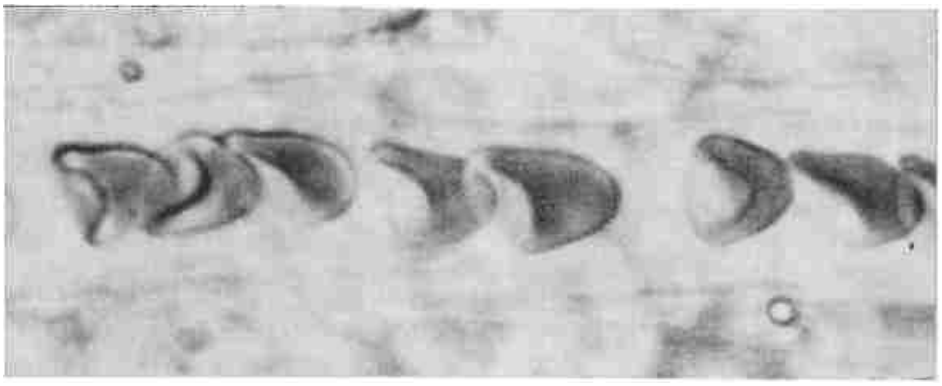

(B)

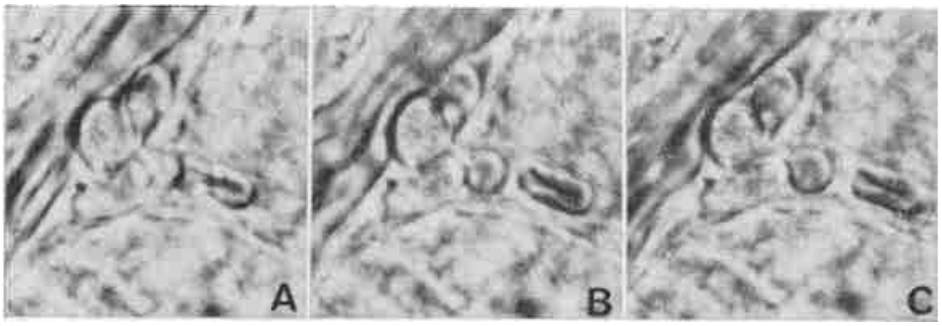

Figure 1.3 Red blood cell deformation in vivo capillary: (a) Cells are squeezing and taking on a parachute-like shape through capillaries of about 7 μm; and (b) Cells are rolling up or flowing at the end of the capillary vessels [5].

The pressure differences, as a result of the diameter changes of the capillary vessels, can cause a local non-uniform stress distribution. Those local stresses generate some deformations of the cell. The experimental results illustrated that if the diameter size of the pore is smaller than 3 micrometers, there is cell damage, and if it is greater than 3 micrometers, the cell remains undamaged [6][13].

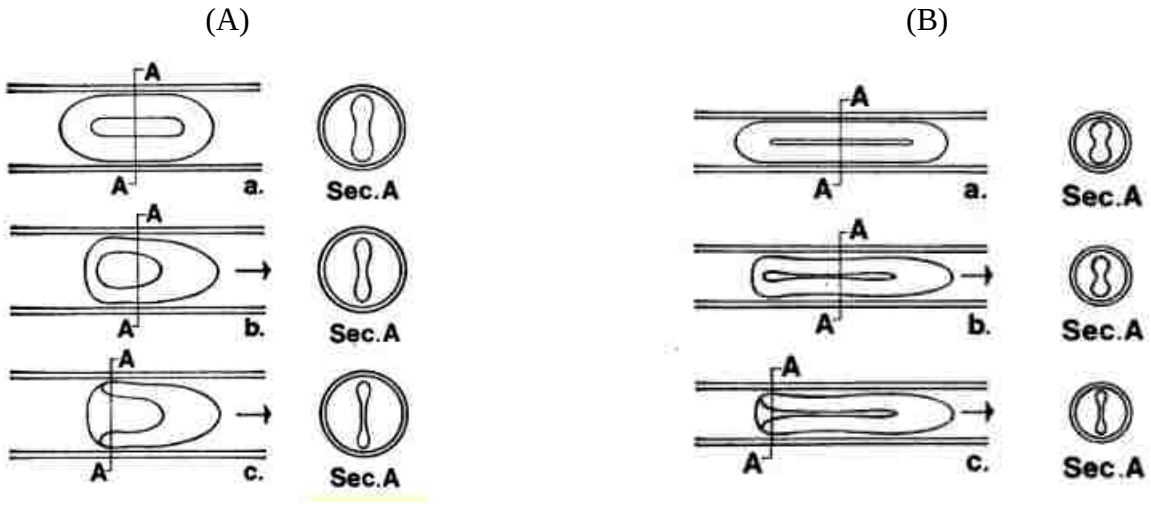

Figure 1.4 RBCs are squeezing through the capillaries: (a) Red blood cell deformation in capillary has a diameter of 7 μm; and (b) Red blood cell deformation in capillary has diameter of 4 μm [5].

The local deformability of red blood cells on high shear stress is essential for observing pore area, rupture, diffusion, and diffusivity. This will allow us to develop our coarse-grained red blood cell patch model, to better understand the mechanical response of various deformable conditions, and to get accurate and detailed answers.

1.2 – Molecular Dynamics

Molecular dynamics technique explores the physical movement of atoms and molecules by Newton's equation of motion respect to time.

$$\vec{F} = m\vec{a} \quad => \quad \vec{F}_i = \frac{\overrightarrow{d_{v_i}}}{dt} \cdot m_i = \frac{d^2\overrightarrow{r_i}}{d_t^2} \cdot m_i \qquad \{1.2.1\}$$

Molecular dynamics methods have been applied in many fields of science including chemical physics, materials science, and the modeling of biomolecules. It is considered a network between the mesoscale and quantum mechanics. Its hierarchic place is presented as follows: (A)

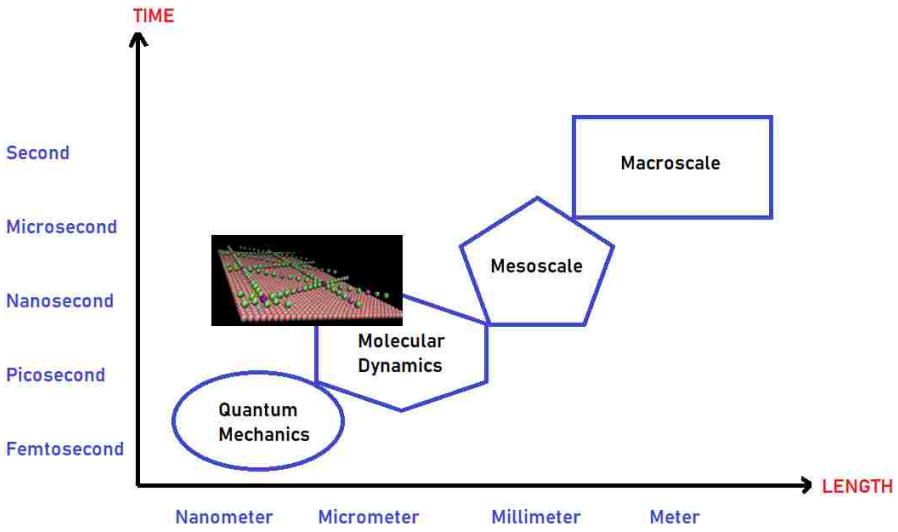

Figure 1.5 (a) Hierarchy of time and length scale simulations.

Quantum mechanics deals with motion and interaction of subatomic particles. Few atoms can be used with the quantum mechanics simulations with the time scale range between femtosecond to picosecond so that its principle can precisely solve any problem, but it is impossible to solve its equations.

The advantage of using molecular dynamics compared to quantum mechanics is that from a few hundred to a few million atoms can be used. In addition to that, by defining some parameters such as the diffusion coefficient, molecular dynamics method yields to couple with finite element method for the simulation of solids or coupling with lattice Boltzmann method for the simulation of soft biological materials or fluidic systems.

The process of molecular dynamics is summarized as follows: in order to have precise macroscale properties, the most significant number of atoms with the accurate time-step selection criteria that is depending on the potentials must be applied to the simulation systems. (A)

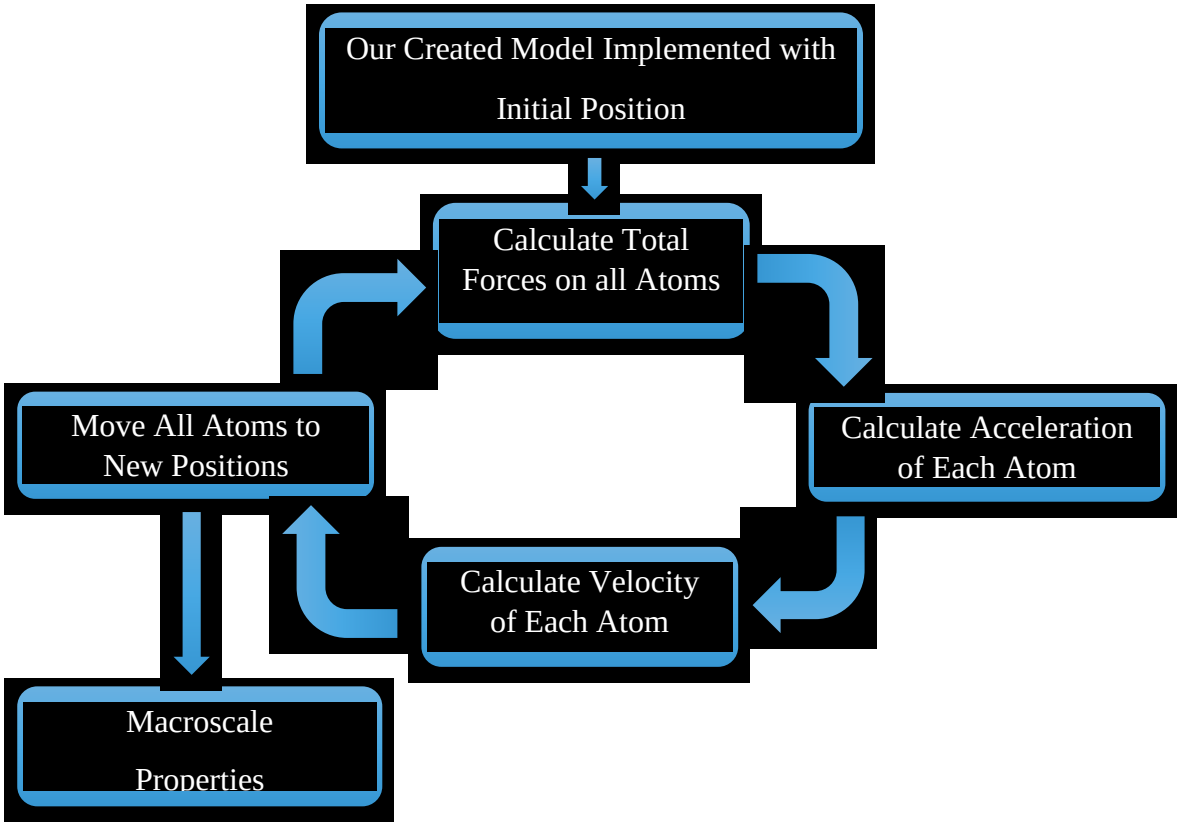

Figure 1.6 (a) Molecular Dynamics Simulation Process: after having positions versus the time, many more macroscale properties can be defined [8].

1.2.1 – Potential Energy Functions

Interactions between particles can be classified into interatomic and intramolecular. By using this interaction, the mechanical properties of the lipid membrane can be captured.

(A)

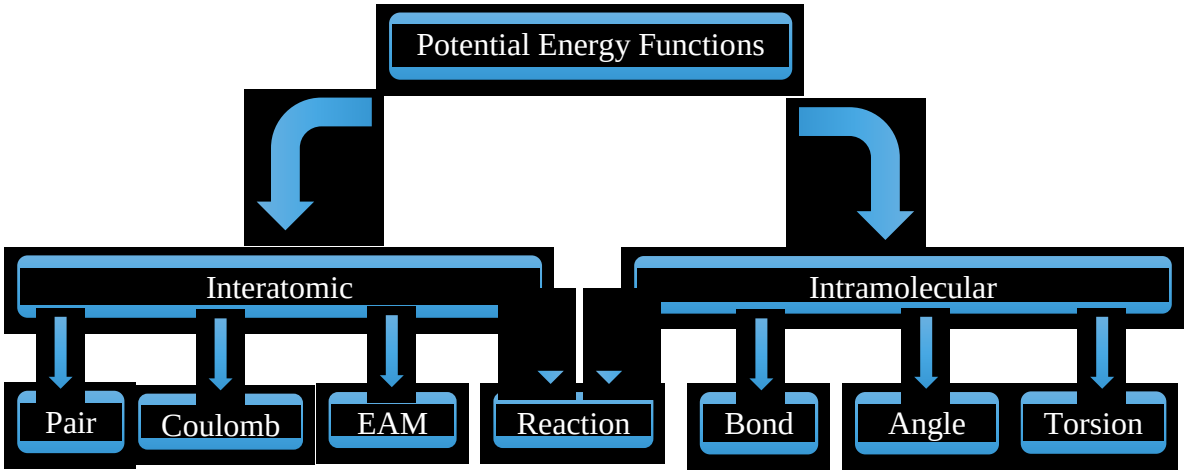

Figure 1.7 (a) Interaction Models to Molecular Dynamics Simulation [9].

Inter-Atomic Potentials as Non-Bonded Forms

Pair potential – The van der Waals interactions can be classified as attraction that act at long distances and repulsions that act at short distances.

In our simulation, we used the Lennard – Jones potentials (n = 12, m = 6):

$$U(r) = k\varepsilon\left(\left(\frac{\sigma}{r}\right)^{n} - \left(\frac{\sigma}{r}\right)^{m}\right) \qquad k = \frac{n}{n-m}\left(\frac{n}{m}\right)^{m/(n-m)}$$

Repulsive **Attractive** {1.2.2}

$$U_{LJ}(r) = 4\varepsilon\left(\left(\frac{\sigma}{r}\right)^{12} - \left(\frac{\sigma}{r}\right)^{6}\right)$$

{1.2.3}

(A)

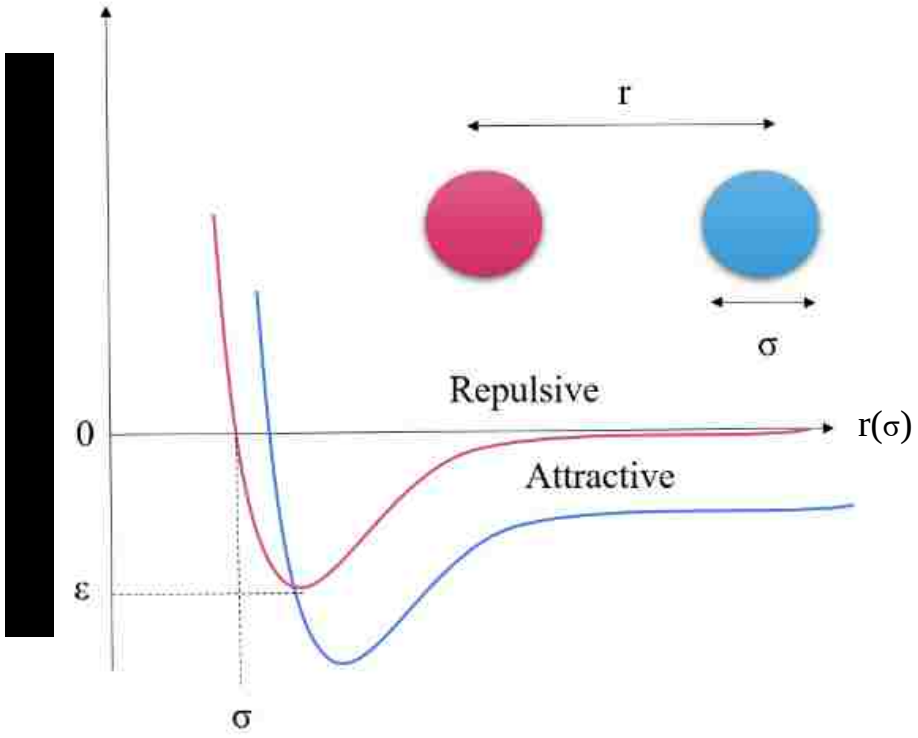

Figure 1.8 (a) Lennard-Jones Pair Potentials

The parameters of pair potentials can be reproduced by either experimental data or accurate quantum chemistry calculations. E is the local minimum of potential energy, σ is referred to as the distance to the point where potential is zero, and r is the distance between the particles.

Coulombic interaction can be included if the electrostatic force between atoms is significant.

Formulation of coulombic is as follow:

$$U_{coulomb} = \frac{1}{4\pi\varepsilon_0}\frac{q_i q_j}{r_{ij}} \quad [9] \qquad \{1.2.4\}$$

q_i and q_j are refered to as atomic charges.

Reactive potentials can also be included along with bond formation and bond disassociation if the system has some chemical reactions.

Intra – Molecular Potentials as Bonded Forms

Bonded potentials functions have distances, angles and dihedral angles as follows:

Bond Stretching Models

$$U_{bond} = \frac{k}{2}(r - r_0)^2$$

$$U_{bond} = D\left[1 - e^{-\alpha(r - r_0)}\right]^2$$

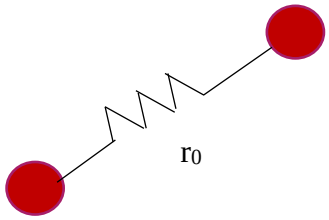

k is a spring constant r_0 refers to bond length. [9]. {1.2.5}

Bond Angle Models

Harmonic angle model

$$U_{angle} = k(\theta - \theta_0)^2$$

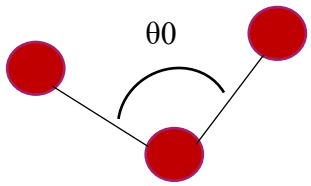

Cosine angle models

$$U_{angle} = k\left[1 + \cos(\theta)\right]$$

k is energy constant and θ_0 is the equilibrium angle [9] {1.2.6}

Torsion Models (dihedrals)

Harmonic torsion angle

$$U_{torsion} = k\left[1 + d\cos(n\phi)\right]$$

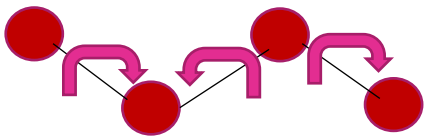

Φ is the angle between two planes [9] {1.2.7}

1.2.2 – Coarse-Grained Patch of Erythrocyte Membrane

Coarse-Grained Modeling is widely used to define the behavior of complex systems such as biomolecules, proteins, cell membranes, and many other molecular level models, and it is crucial to solving time-scale and length-scale problems [7]. A patch of human red blood cell is modeled by using molecular dynamics, but not all-atom methods. Therefore, we need to reduce the scale of representation to avoid sizeable computational time. To do that, we placed a group of atoms into a coarse-grained bead, which is also called a pseudo-atom model. Before building our own the coarse-grained bead model, we will carefully look at the erythrocyte membrane components. The erythrocyte membrane mainly consists of the spectrin network and a phospholipid bilayer. The spectrin network forms consist of spectrin tetramers tethered to the membrane at the junctional complex (actin), ankyrins, and band-3 proteins.

(A)

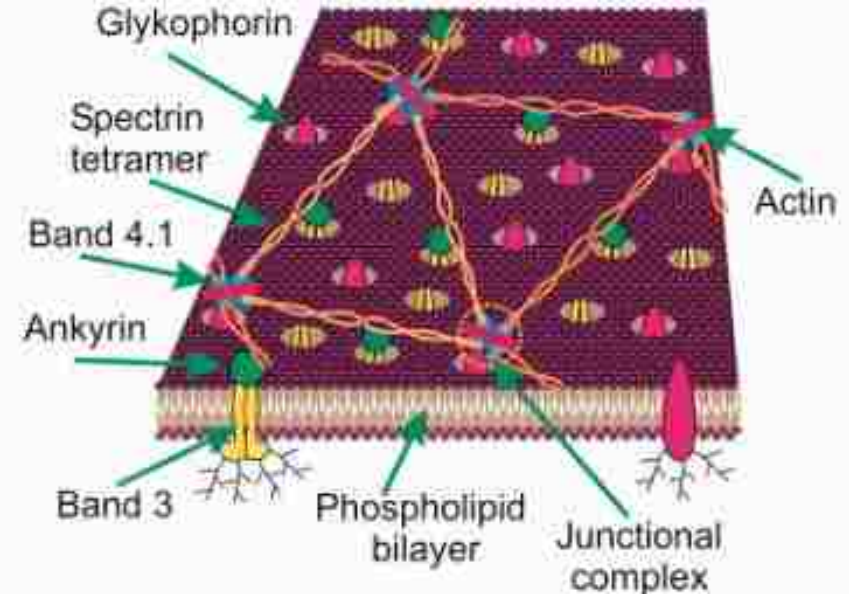

Figure 1.9 (a) Schematic of the cytoskeleton of the patch of human red blood cell [10].

A two-component model is built up to simulate two main components of the erythrocyte membrane, the lipid bilayer, and the spectrin network, separately [10].

Lipid bilayer resists bending and has a large local area stiffness but cannot undergo in-plane shear stress because the lipids potential is not as strong as spectrin network and most of the proteins can diffuse freely within the membrane to relax the shear stress [11]. Each spectrin tetramer has intertwined and antiparallel α-spectrin and β-spectrin filaments.

(A)

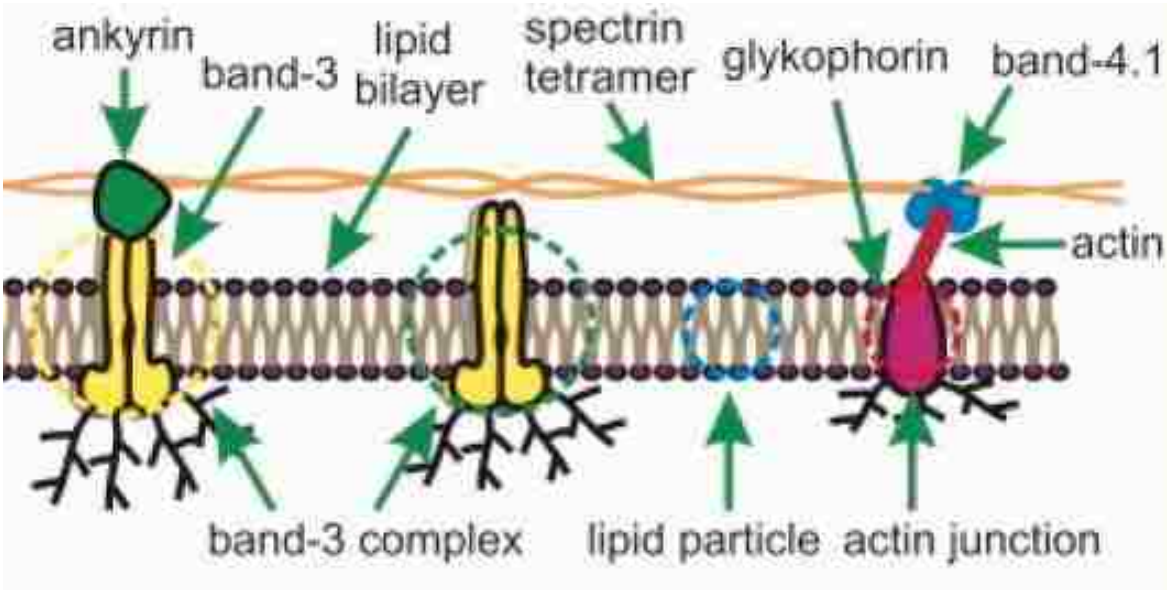

Figure 1.10 (a) At the first yellow circle, band-3 complex connected to the spectrin network, band-3 complex illustrated at second green circle by connecting spectrin tetramer as well. Blue circle third marks a group of lipid particle, and on the fourth circle actin junction connected to the band -4.1 [11].

Now, we will build a coarse grained model which consists of the lipid membrane, spectrin network, actin junctions, band-3 complexes.

Chapter II. CGMD MODEL FOR A PATCH OF A HUMAN RED BLOOD CELL

2.1 – Lipid Membrane

In our model, the lipid membrane is modelled with coarse-grained particle beads. A group of lipid molecules are inserted (A) into a bead (B) with a diameter of 5 nm.

(A) (B)

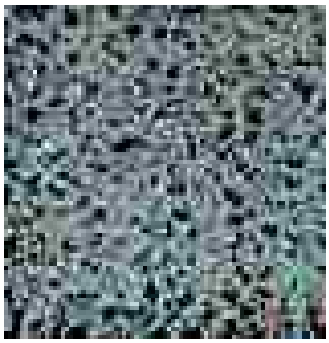

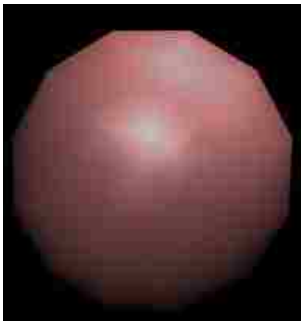

(C)

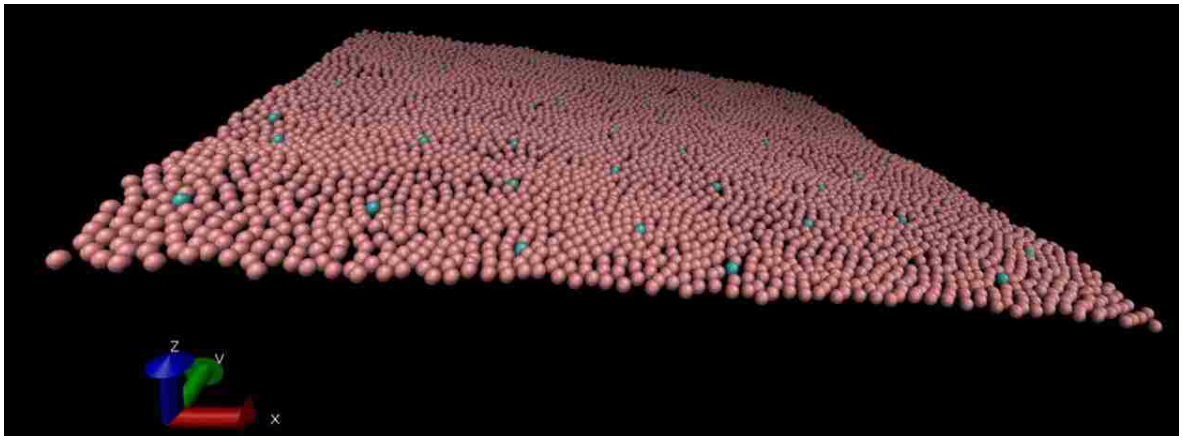

Figure 2.1 Construction of the hierarchic model for the lipid membrane of a human red blood cell. (a) The lipid bilayer is represented as the full atomistic model. (b) The mesoscale coarse-grained bead from the lipid bilayer has a diameter of 5 nm. (c) The patch of the erythrocyte membrane is made of mesoscale beads. Blue mesoscale beads represent the parts of either actin junctions or transmembrane proteins.

2.2 – Spectrin Network

The structural model of the spectrin networks has three coarse-grained components. The first one is a bonded bead that is composed of spectrin tetramers. Second, the transmembrane protein is a combination of two beads wherein one bead is in the middle of the spectrin network and another bead is inserted just below its couple ones on the membrane. Third, the actin junction consist of two beads wherein one is located in the middle of the hexagonal network and another is oriented perpendicular to the membrane.

Tetramers are connected at the actin junctional complexes by combining a hexagonal network with 39 beads, but transmembrane proteins on tetramers represent different types due to being bonded with membrane beads as well. The remaining spectrin beads are linearly connected with adjacent ones by bonds. Besides those, whole spectrin beads are assigned with varying numbers of types to implement interaction potentials.

(A)

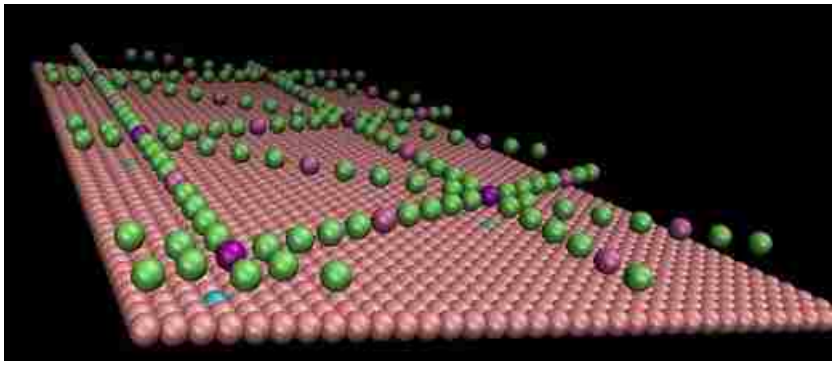

Figure 2.2 (a) Spectrin network are encoloured as purple, green and light purple beads. Purple beads are connected to both green beads and actin junctions which are blue beads. Light purple beads are bonded to both transmembrane proteins and green beads. The remaining green beads are bonded to entire adjacent ones.

(A)

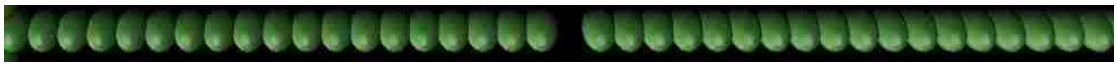

(B)

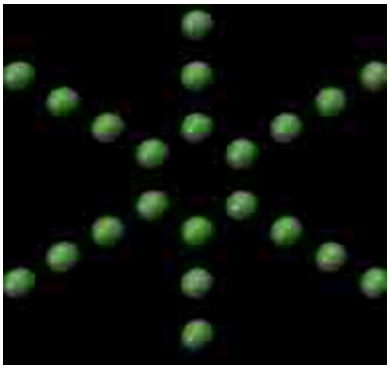

(C)

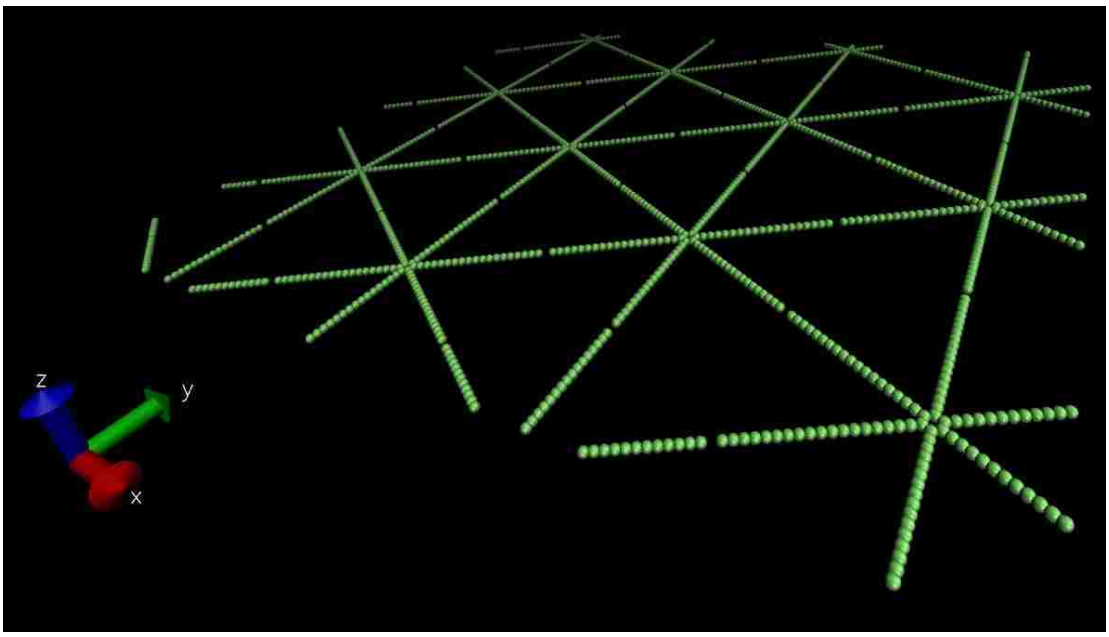

Figure 2.3 Coarse-grained particle model of the spectrin network. (a) Spectrin filament with 39 beads connected by bonds. (b) The six-fold structural unit of the spectrin network. (c) The spectrin network.

2.3 – Transmembrane Proteins and Actin Junctions

Transmembrane proteins, known initially as band-3, are made up of a couple of light purple and blue beads in our model (a) and are located on the middle of the spectrin filaments and perpendicularly on the membrane. We used unique types of those beads to connect the lipid bilayer by with relative Lennard-Jones potential and to connect spectrin filament beads with a weak harmonic bond.

The actin junctions are connected to the lipid bilayer via glycophorin. (b) In our model, we had two actin junctions made up of one light purple bead and one blue bead. Connections between the actin junctions located on the spectrin network and the lipid membrane are represented by a relatively weak LJ potential, and a weak harmonic bond. Each actin junction's bonds are not only connected to membrane proteins but to hexagonal networks, as well.

(A)

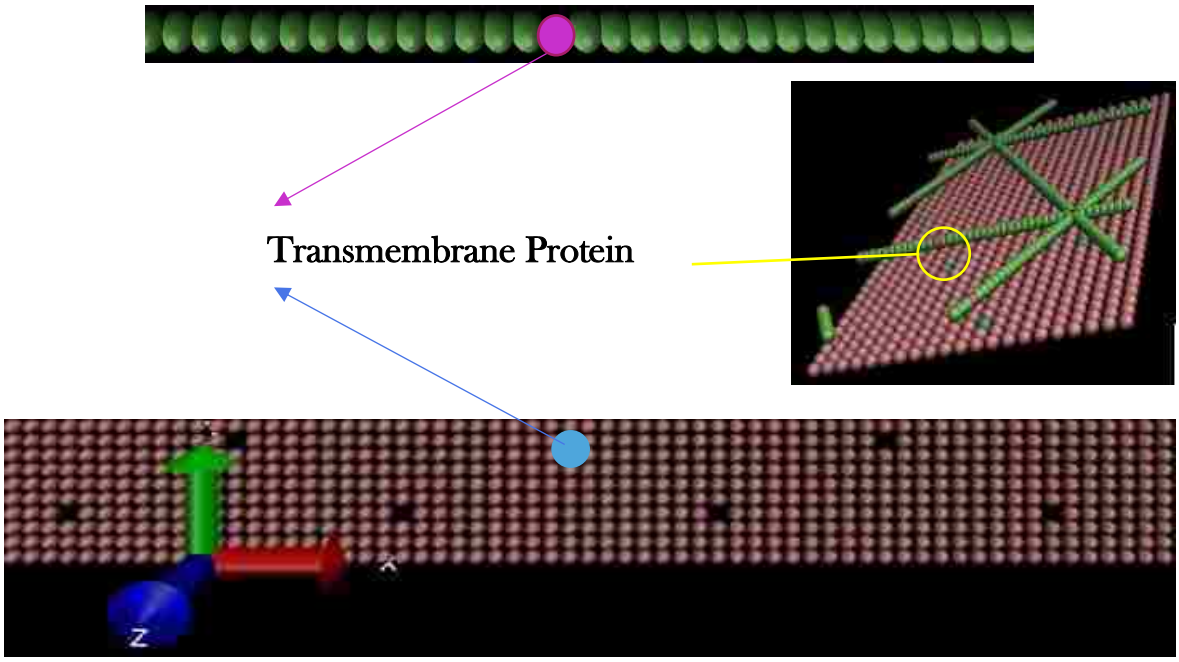

(B)

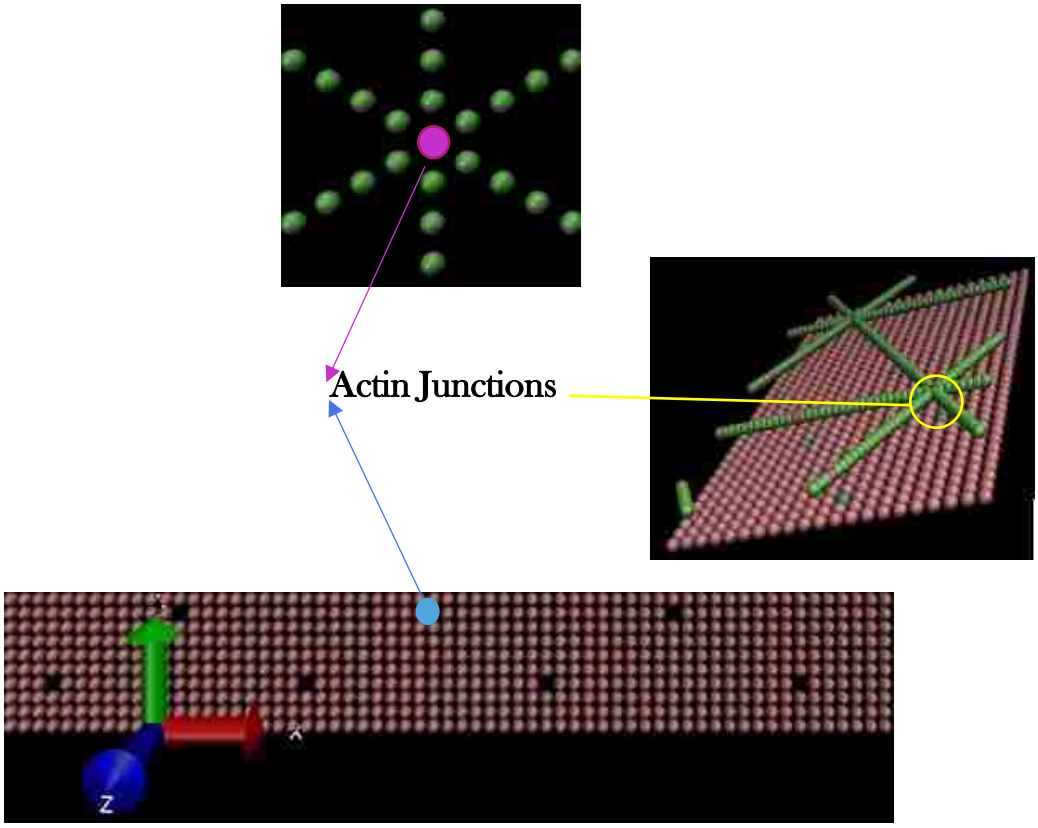

Figure 2.4 Transmembrane proteins and actin junctions' places on the spectrin network and lipid membrane, respectively. (a) Transmembrane protein located on the middle spectrin filament along with 39 beads and a lipid membrane. (b) Actin junctions are placed on a hexagonal spectrin filament by bonding 6 green beads to the lipid membrane.

2.4 – Force Fields and Simulation Setup

Seven-atom types were used in our model; lipid membrane beads, actin junctions, combinations of two types of beads, transmembrane proteins divided into two types, a spectrin network, and water molecules as six layers located downwards of the spectrin and upwards of the lipid membrane.

The repulsive potential is used to define interactions between non–bonded actin junctions with the hexagonal spectrin network and lipid membrane' beads. The interaction between the spectrin network and the lipid membrane are quite weak, as represented by LJ potentials. To simulate LJ in LAMMPS, we need to define some main parameters:

ϵ (Kcal/mol), σ (Angstrom), r_c (Angstrom).

For bonded potentials, we used bonds between the transmembrane proteins of spectrin, middle particles of spectrin and actin junctions. The main parameters are given in **Table 2.1** as non-bonded and bonded parameters obtained from Fu et al. [12].

Table 2.1 Potential parameters for the system

Non – Bonded Potential Parameters	ϵ (Kcal/mol)	σ (Angstrom)	τ
Membrane beads	0.269 kcal/mol	5 nm	0.1 μs

Bonded Beads	K (Kcal·mol^{-1}·A^{-2})	r_0
Middle particles of spectrin.	300	7.6 (A)
Spectrin heads and actin junctions.	200	7.6 (A)
Middle particles and head particles of spectrin.	300	63.8 (A)

The non-bonded terms for force fields can be expressed as:

Spectrin particles that are not connected by the spring potential which interact with each other via the repulsive part of the L-J potential as follows:

$$U_{non-bonded} = U_{LJ}(r) = 4\varepsilon_{ij}[(\frac{\sigma_{ij}}{r})^{12} - (\frac{\sigma_{ij}}{r})^{6}] \quad \{2.1.1\}$$

In the formula, σ_{ij} denotes the closest approach between two particles, and ε_{ij} represents the strength of their interaction, and only one type of bond is used in the spectrin tetramer interaction between the middle particles of spectrin, middle particles and head particles of spectrin and spectrin heads and actin junctions.

The total energy of bilayer beads can be summarized as:

$$U^{total\ energy} = \sum_{ij}^{n} 4\varepsilon[(\frac{\sigma}{r_{ij}})^{12} - (\frac{\sigma}{r_{ij}})^{6}] \quad \{2.1.2\}$$

Compared to the lipid membrane, the spectrin network's bonds are stronger than non-bonded membrane beads. That is why, in our rupture analysis, we recognized this weakness by observing small pore deformation on the membrane before the patch completely ruptured.

The bonded interactions included harmonic forms and angles with weak harmonic potentials

$$U_{bond} = \frac{1}{2}K_{bond}(R - R_{bond})^2 + \frac{1}{2}K_{degree}[cos(\theta) - cos(\theta_0)]^2 \quad \{2.1.3\}$$

Although LAMMPS has harmonic functions that can represent all beads bonds, we obtained our revised harmonic functions from Fu, Peng, Yuan, Kfoury, and Young's, (2017) paper by implementing some parameters [12].

2.4 – Simulation Setup

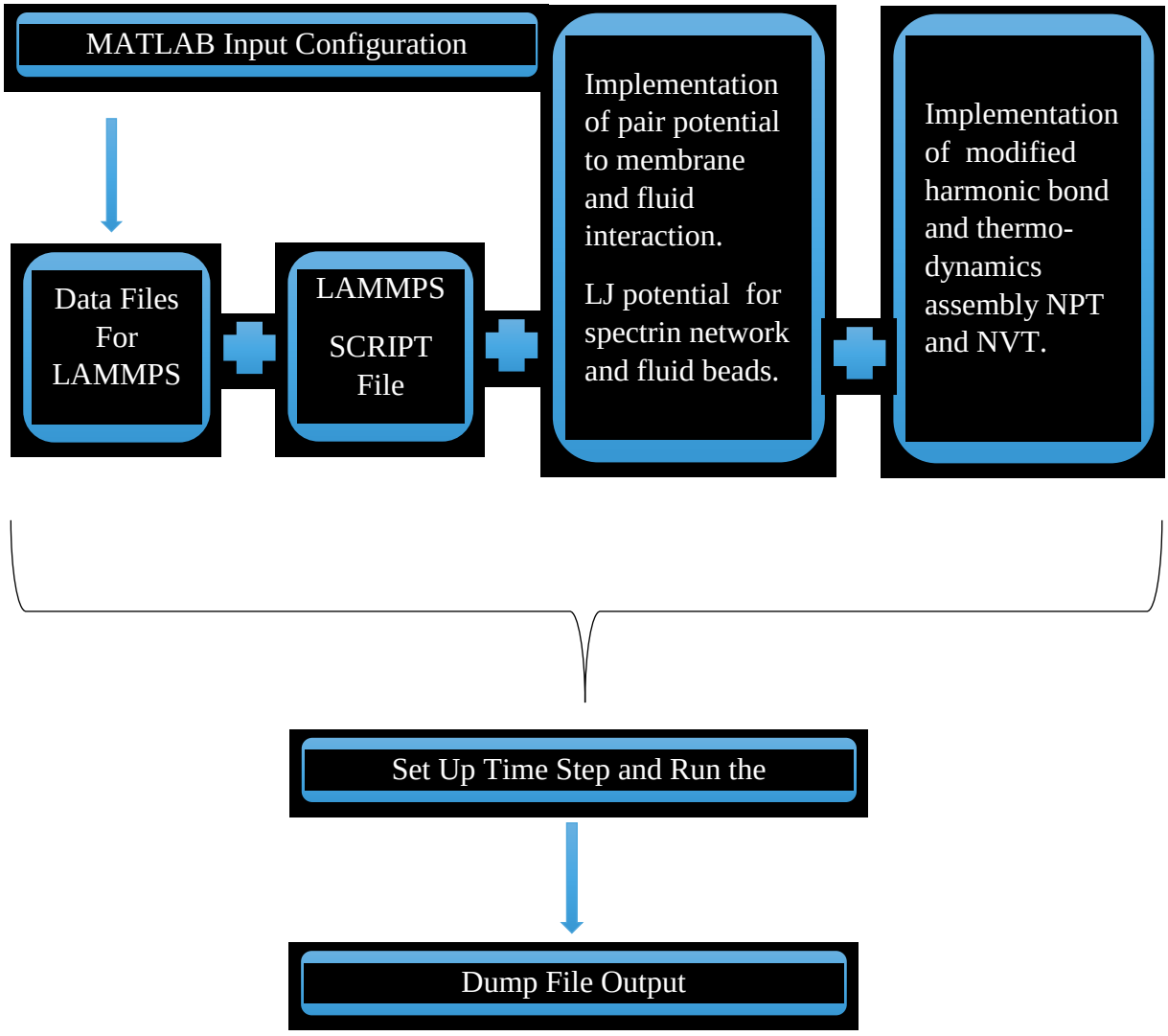

Figure 2.5 Flow of our simulation process on LAMMPS [12].

2.5 – Patch of a Human Red Blood Cell Modelled on MATLAB

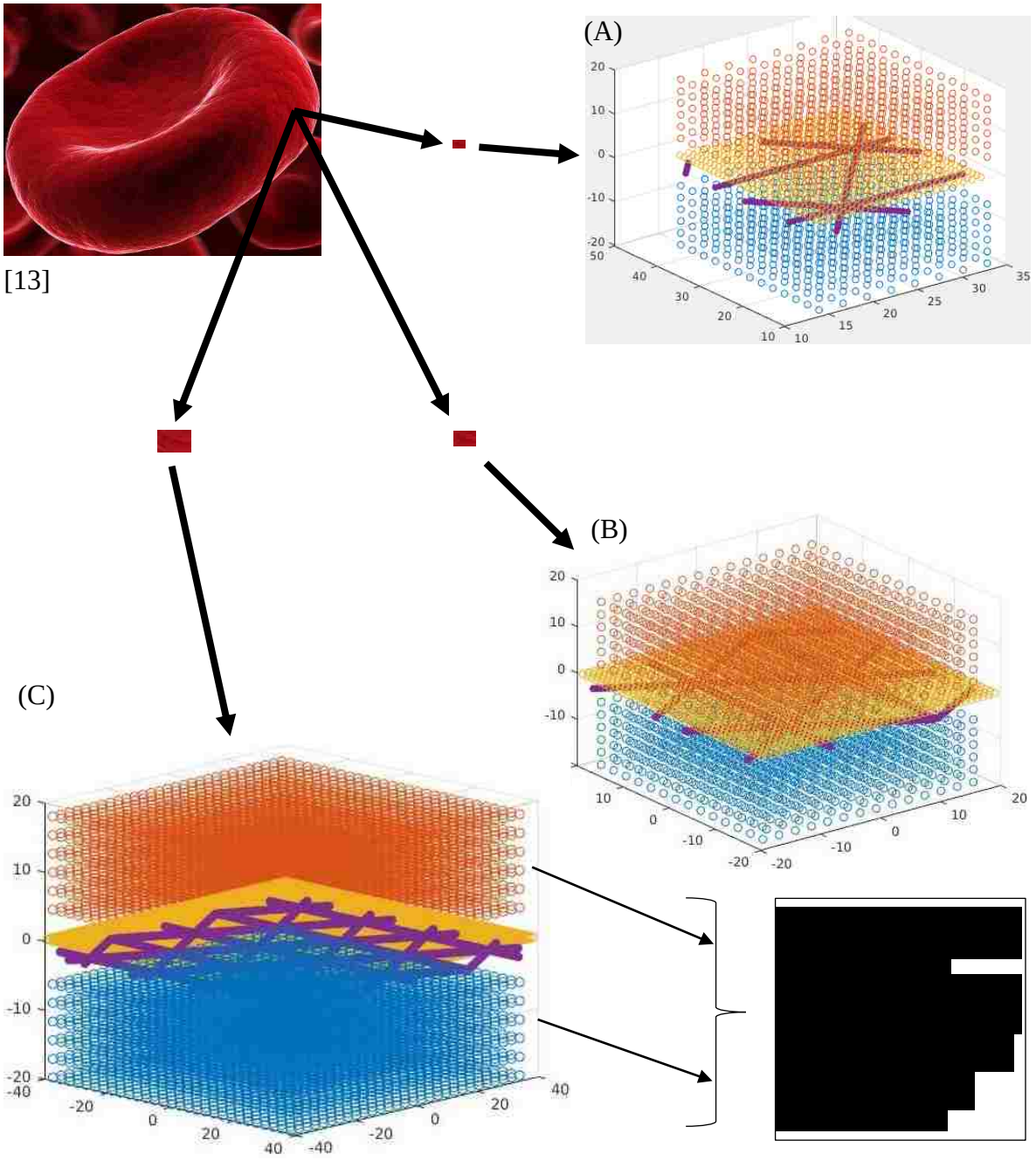

[13]

Figure 2.6 A human red blood cell [13] and our patch models created MATLAB.

(a) The smallest patch size of 30 x 20 nm (b) Size: 40 x 40 nm (c) Size: 80 x 80 nm.

2.5 – Patch of a Human Red Blood Cell Modelled on LAMMPS

(A)

[13] 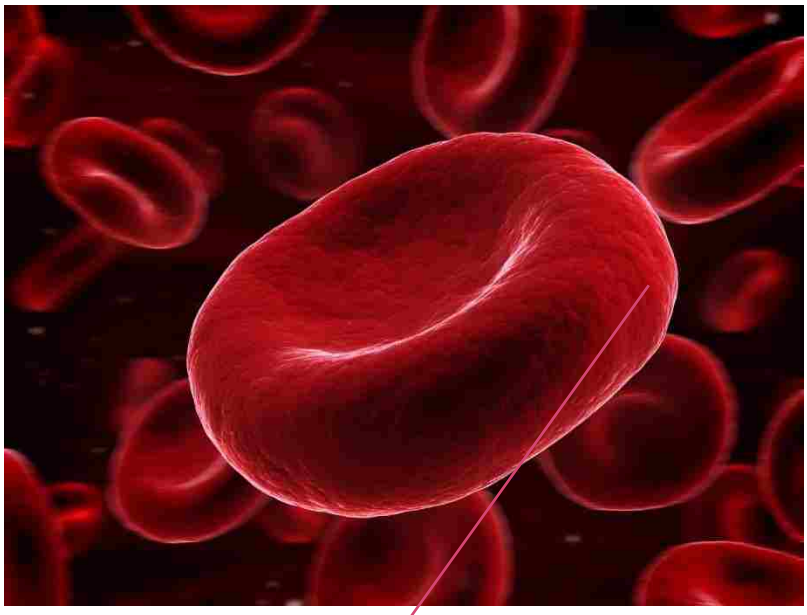

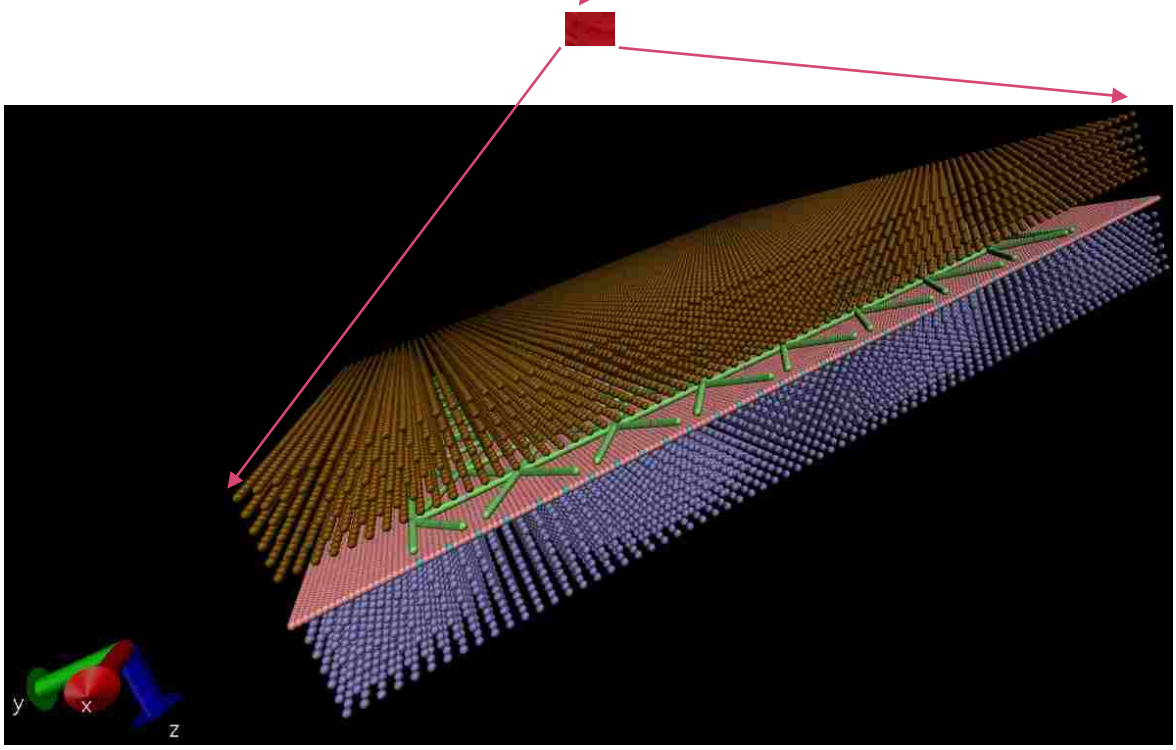

Figure 2.7 A human red blood cell [13] and our patch model created on LAMMPS.

CHAPTER III. RESULTS, CONCLUSION AND FUTURE WORK

3.1 – Membrane Diffusion and Diffusivity

Having obtained and applied paired potentials for coarse-grained lipid molecules, we are able to model the diffusivity properties of the patch of red blood cell. One of the main reasons we analyze the diffusion property of the patch is to define the diffusion coefficient value the and type of diffusion regime.

We found the diffusion coefficient value to be $D \approx 2.4624\ \mu m^2 s^{-1}$ which can be obtained by taking an average of diffusivity from time step 200 to 1000 microseconds. Auth et al. calculated that the diffusion coefficient of the lipid membrane is $D \approx 1\ \mu m^2 s^{-1}$ [14].

The diffusion coefficient is known to depend on the surface tension. Furthermore, Auth & Gov (2009) found that the density of the anchor point results in pressure differences in the cytoskeleton that can cause a different diffusion coefficient together with different degree of stretching [14].

Our modeled membrane's dimensions are: 71σ x 56σ (σ=5nm), and the number of particles is 3,976 beads. We performed constant NVE integration with the MSD LAMMPS command. The Mean Squared Displacement is formulated as:

$$MSD \equiv \langle (\chi - \chi_0)^2 \rangle = \frac{1}{N} \sum_{n=1}^{N} (x_n(t) - x_n(0))^2$$

N represents the total particles in the system, and χ and χ_0 refer to the position of each particle. When we add time, which is $x_n(t)$, we can determine the position of the particle for our desired time.

(A) (B)

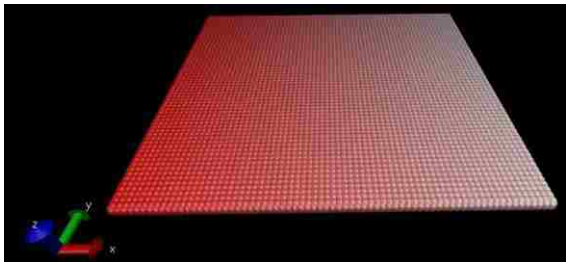

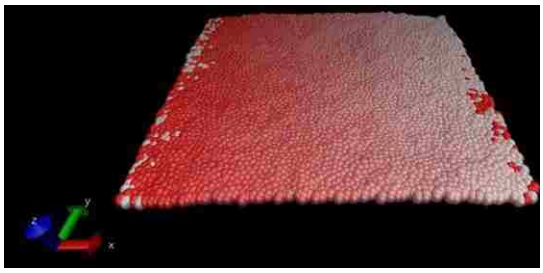

(C) (D)

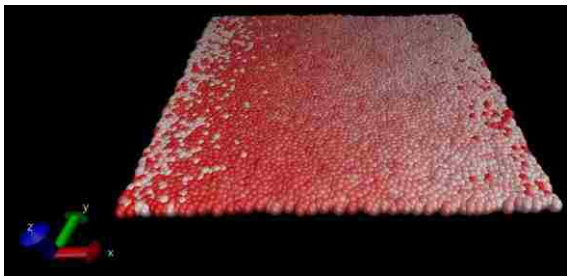

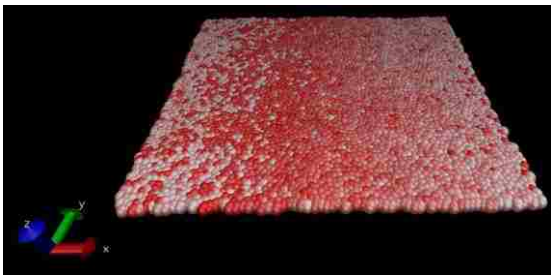

(E) (F)

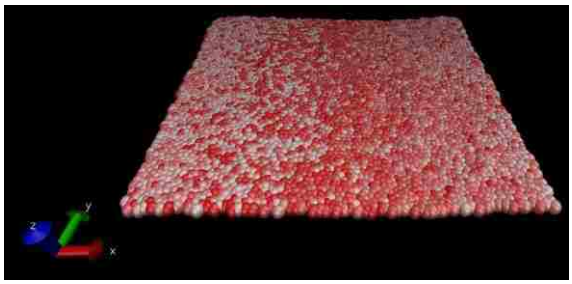

Figure 3.1 Snapshots taken from A to F illustrate membrane diffusivity configuration at different time steps (a) Initial state of red blood cell membrane where color transition is represented in red and white. (b) Diffusivity dispersion at the time step 200 microseconds (c) Diffusivity dispersion at the time step 400 microseconds (d) Diffusivity dispersion at the time step 600 microseconds (e) Diffusivity dispersion at the time step 800 microseconds (f) Diffusivity dispersion at time step 1,000 microseconds.

(A)

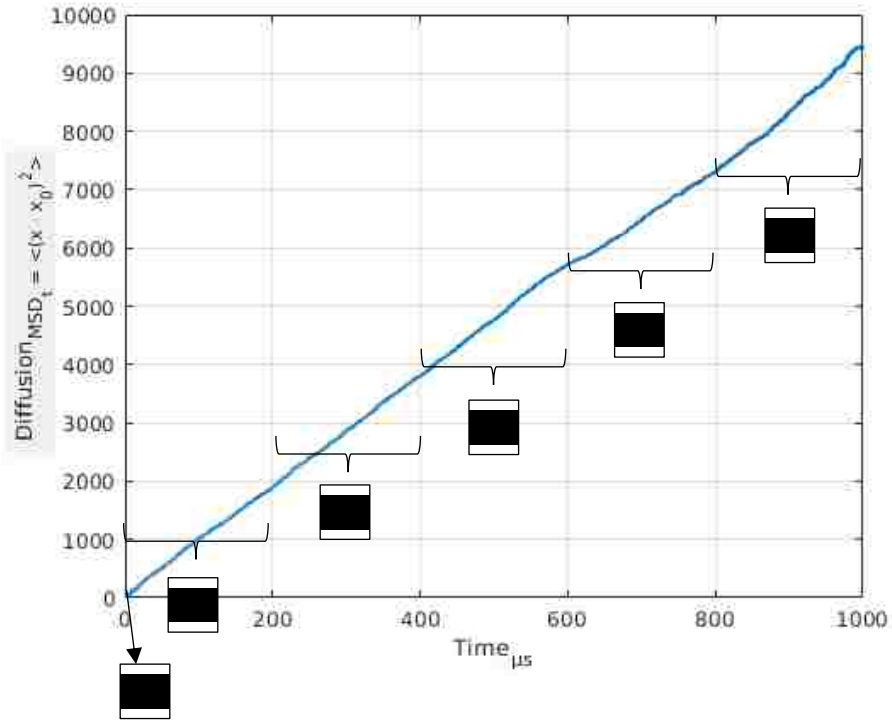

Figure 3.2 (a) Diffusion property of patch of human Red Blood Cell membrane versus time; rectangle A is located very close to zero point and its time just first microsecond at the beginning of the simulation. Rectangles from B to F are shown as have 200 microseconds time range.

(B)

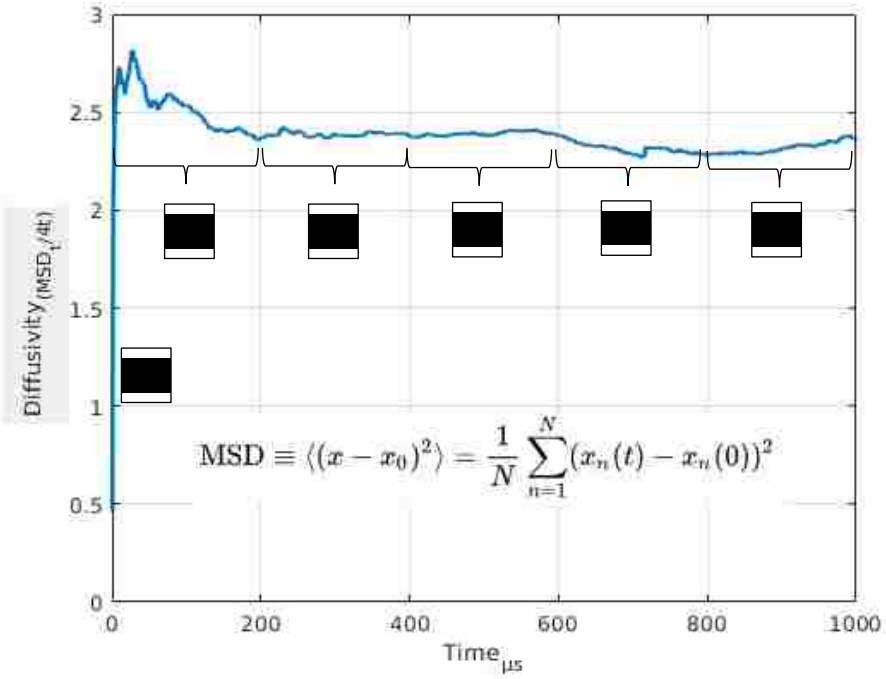

Figure 3.2 (b) Diffusivity versus time: At the ultra-short time what is first micro-second particle do not interact with each other. This time observes as almost vertical slope goes 0.5 to 2.6. From 0 to 200 microsecond the system can stay at stable stage, which means when the simulation is run; it can't start at the beginning of the equilibrium stage. After the 200 microsecond, beads behave like a fluidic structure and they travel randomly both from boundary and through the membrane.

3.2 – Mechanism of Rupture of the Patch of RBC and Membrane Tension

In this part, uniaxial tensile stress applied to patches of red blood cell and rupture mechanism was explored. Then, the critical stress/strain analysis was compared to experimental results.

Raucher and Sheetz experimentally stretched membrane-attached beads with uniformly using laser tweezers [17]:

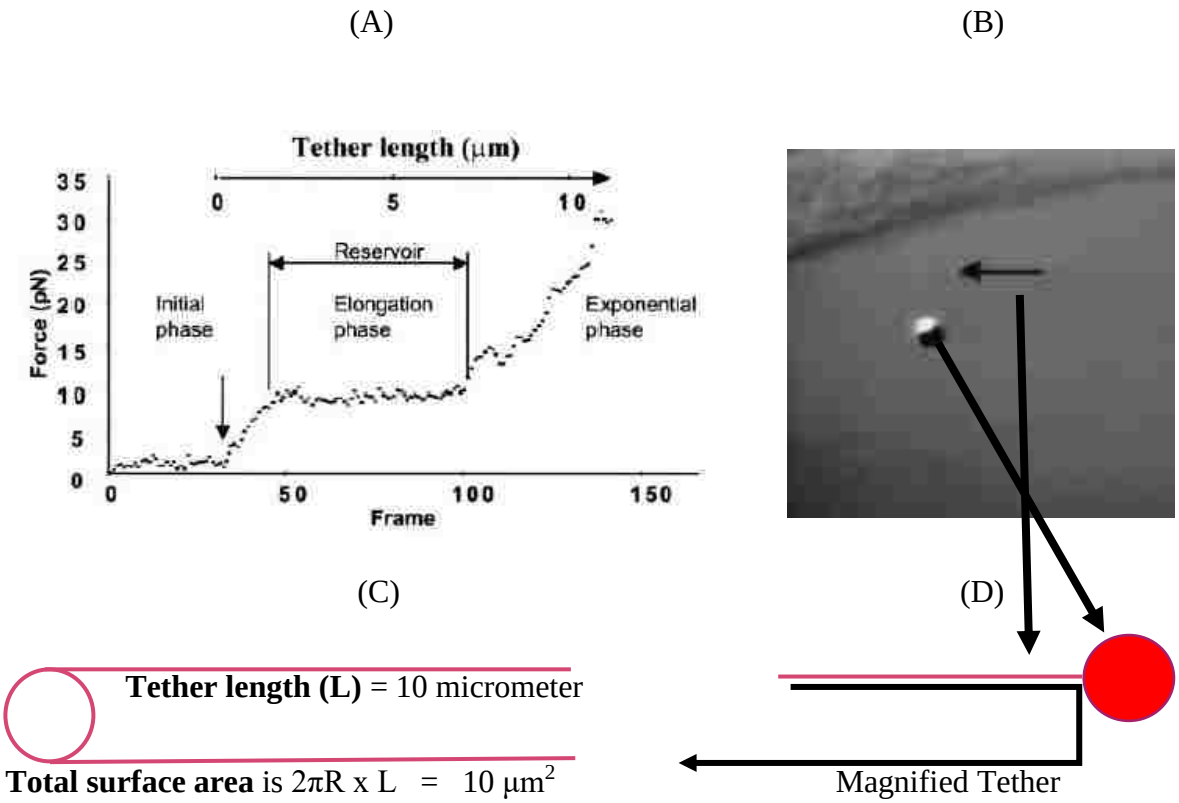

Figure 3.3 (a) Tether formation phases are given with time versus frame[17]. (b) Membrane tether was formed by stretching out the bead[17]. (c) Total surface area of the stretched bead. (d) Schematic figure of red blood cell with its stretched bead.

In this model, the patch is built with the total area of 10^3 nm^2 and then the lipid membrane and spectrin network were stretched with uniformity until the patch completely ruptured. Maximum stress at the breakable point is found as 2.5 x 10^{-5} GPA. We need to convert this result to pN which will enable us to compare the result with experimental data.

The GPA can be expressed to pN by using a mechanical SI derived unit as follows:

$$1\ GPA_{Gigapascal} = 10^9 \left(\frac{1\ N}{m^2}\right)\left(\frac{10^{12}\ pN}{1\ N}\right)\left(\frac{1\ m^2}{10^{18}\ nanometer^2}\right) \quad \{3.2.1\}$$

After reducing this expression, we have:

$$1\ PicoNewton = 10^{-3}(GPA\ x\ nanometer^2) \quad \{3.2.2\}$$

If we multiply the breakable point by total area, we get 2.5 x 10^{-3} $(GPA\ x\ nanometer^2)$ This result equals 2.5 pN force.

Simulation snapshots and results are given as follows:

(A)

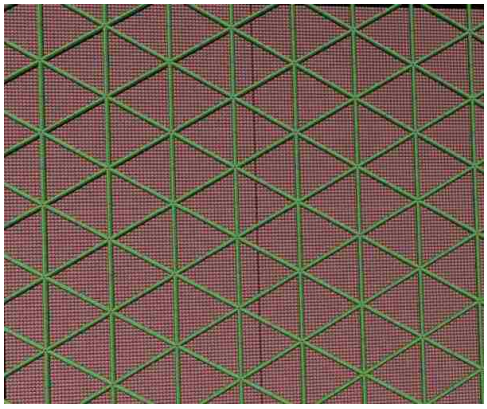

(B)

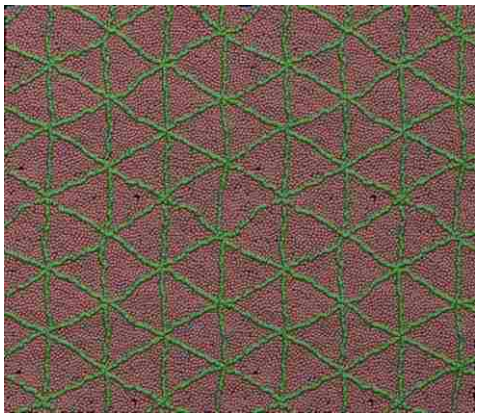

(C)

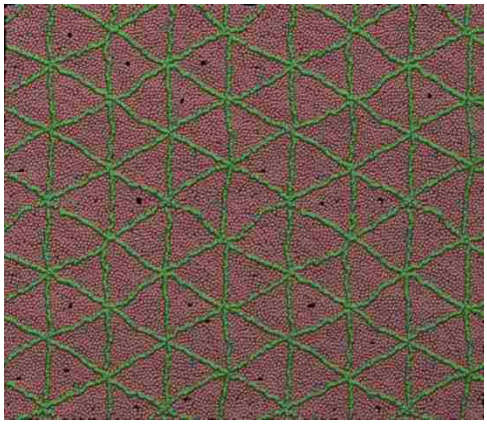

(D)

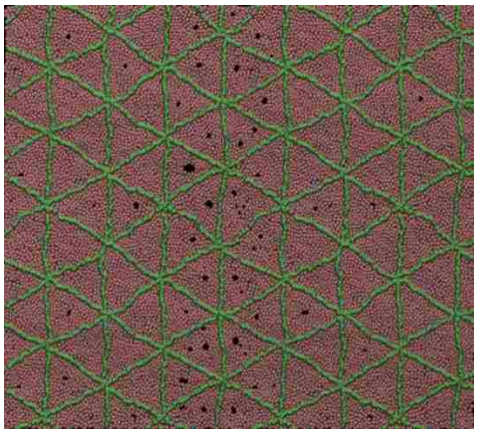

(E)

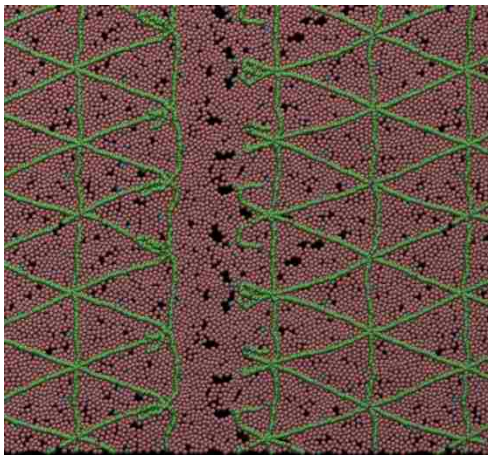

(F)

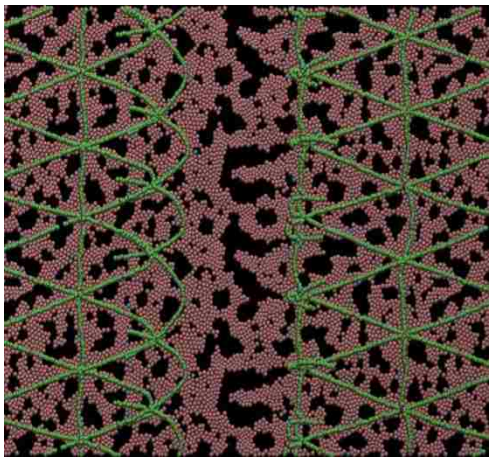

(G)

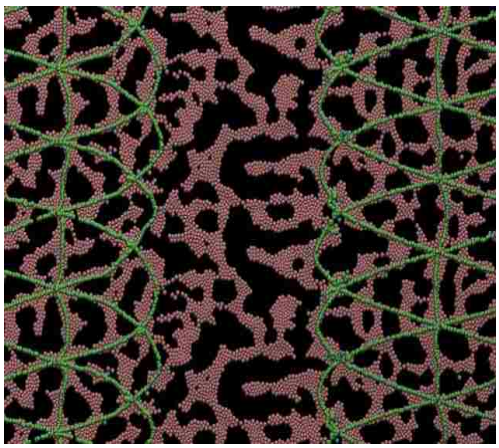

(H)

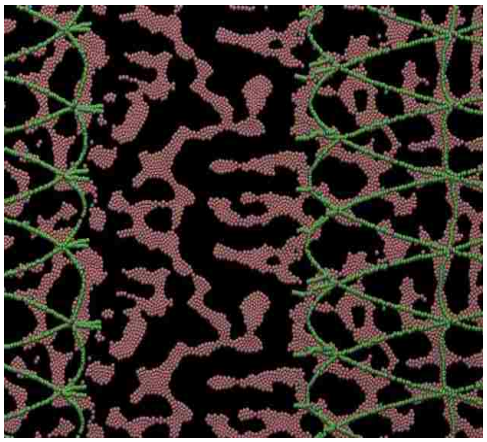

(I)

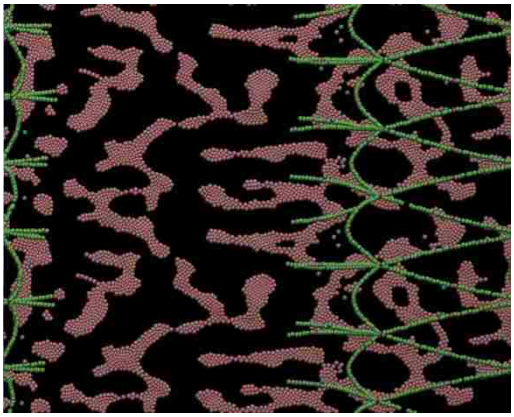

Figure 3.4 Rupture mechanism for the patch of human erythrocytes membrane is given in here as snapshots created on LAMMPS. (a) The initial condition of the lipid membrane with spectrin network is shown. (b)(c)(d) From B to D, first, a small pore formation is observed, and then those pores are increased both in size and number, respectively. (e)(f)(g)(h)(i) At the E snapshot, the simulation reached the breakable point, and the patch was ruptured. After E, dispersion of the fragmental lipid membrane and spectrin network's motion is observed.

(A)

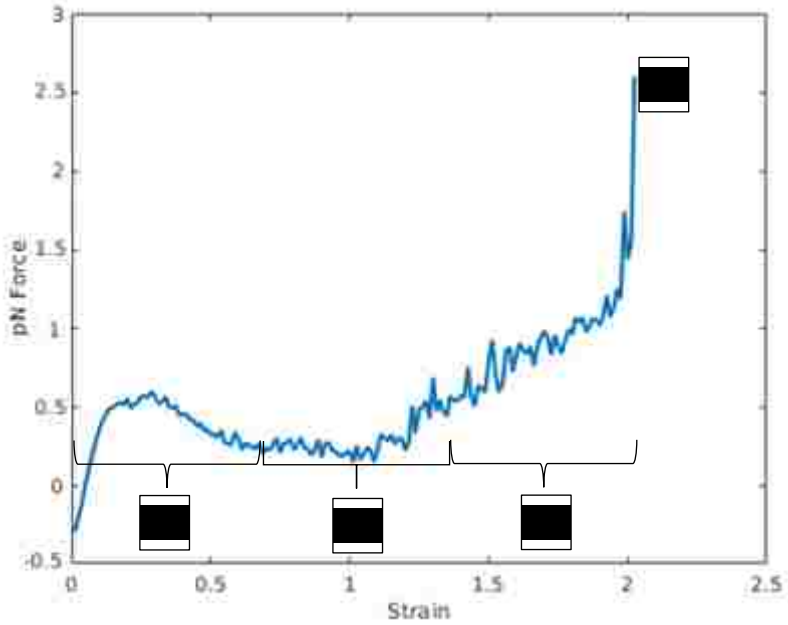

Figure 3.5 Uniaxial tensile stress is applied until we reach the membrane-spectrin final rupture point to determine the ultimate force. Rectangle marks; A, B, C, and D, are given in order to illustrate the different stages of the snapshots on the patch of the membrane as a result of pulling forces. (A) Entire pulling forces are determined until the force reaches to membrane breakable point.

After dividing surface force which are obtained in experiments in laser optical tweezers trapping a bead to the length of circular tether membrane given at **figure 3.6 (a)** and dividing surface force to the length of our modeled patch along which the force acts given at **figure 3.6 (b),** we define the surface tension to compare.

The surface tension equation is given by:

Surface Tension = [surface force] / [length force acts]

(A)

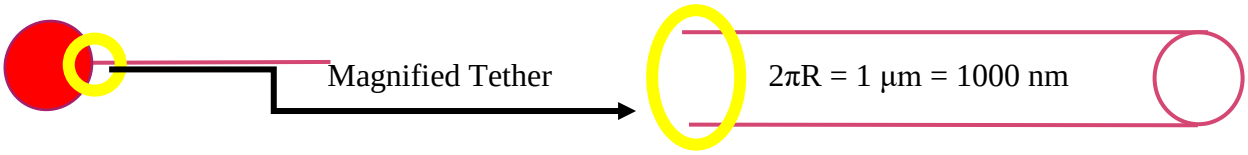

Surface Tension = F / 2πR

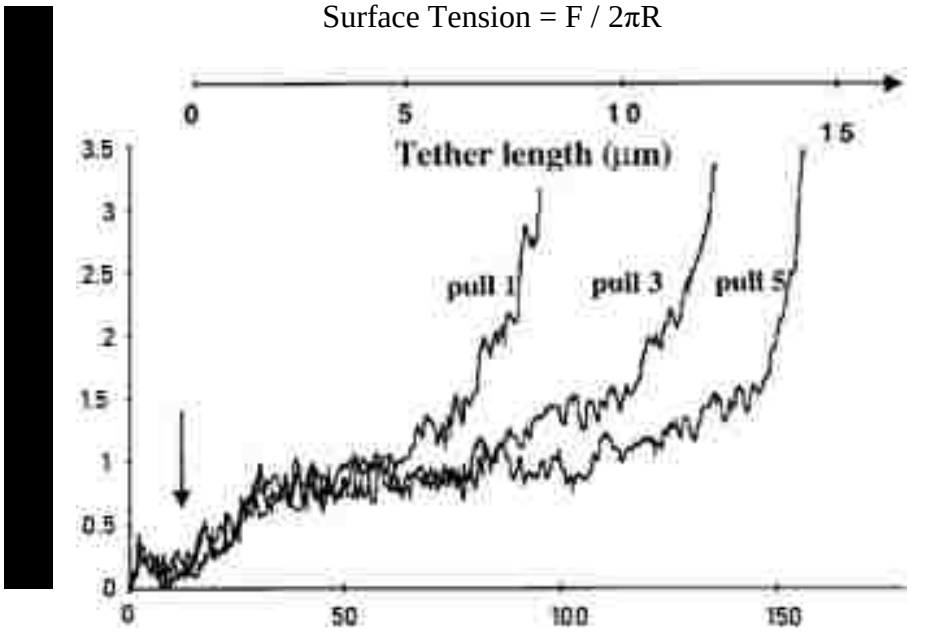

[17

(B)

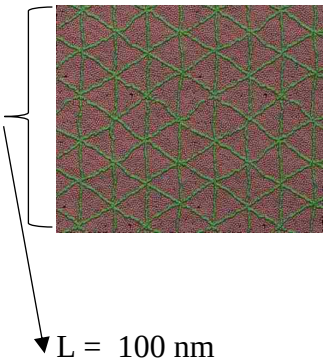

L = 100 nm

L = 0.1 μm

Surface Tension = F / L

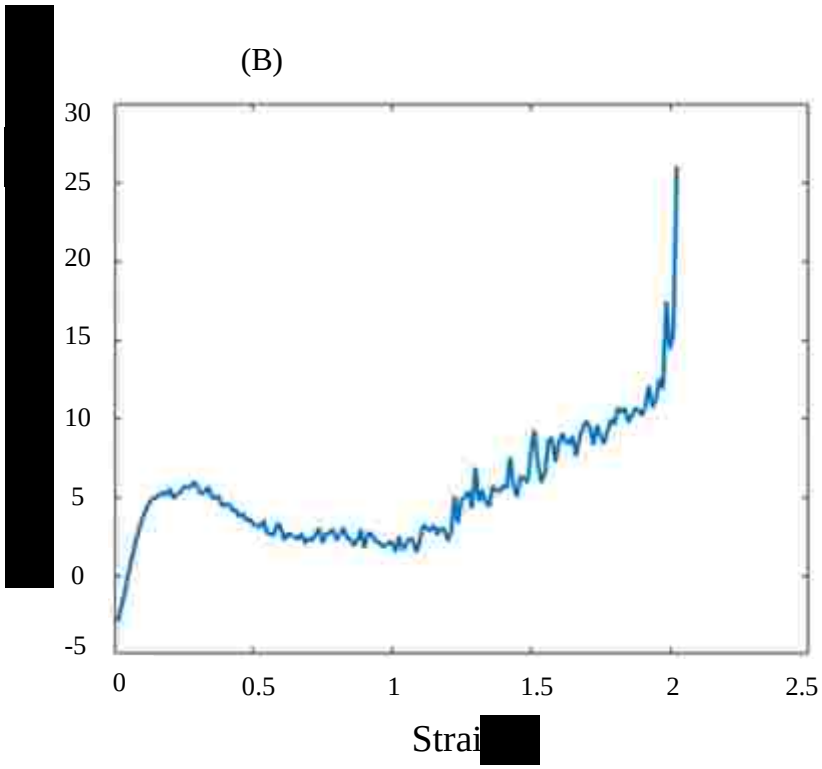

Figure 3.6 (a) Surface tension is given with several tether deformations revised by paper[17] graph, and (a) The surface tension is defined to the length (L) of our modeled patch along which the force acts.

(A)

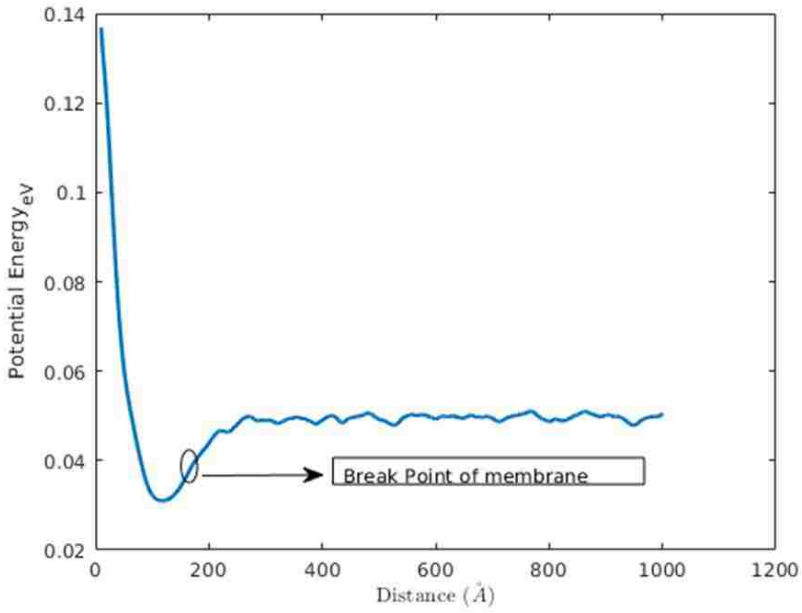

Figure 3.7 (a) Energy vs. distance graph. The breaking point of the membrane-spectrin network is illustrated here inside the black circle.

3.3 – The Pore Area of the Patch of Erythrocyte Membrane at the High-Stress Region

Shear induced single cell has been well studied in literature in order to obtain some mechanical properties. Nevertheless, the coarse-grained model as a patch has not yet been analyzed. Looking at the velocity field around the cell illustrated in **Figure 3.5 (A)**, we encounter some stagnation points that exist during the motion of shear flow. In that region, shear forces lie symmetrically to opposite sides. Abkarian and Viallat [18] illustrated that highest stress distribution exists in that region. After determined this area, we applied shear force on our patch model which is in **Figure 3.5 (B)** to further and with greater define pore formation.

(A)

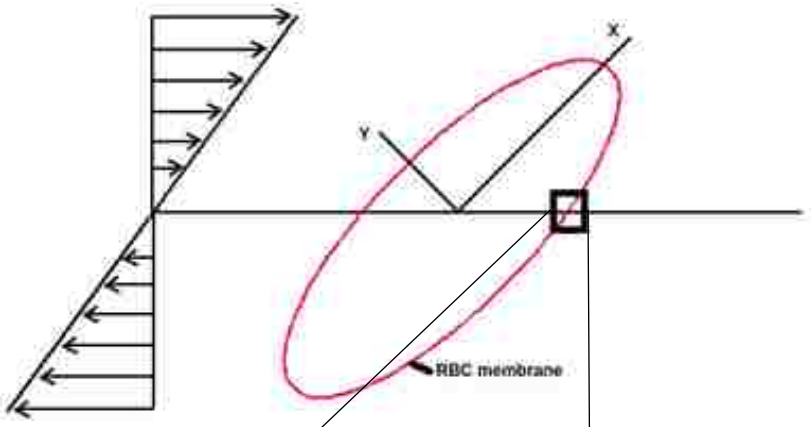

(B)

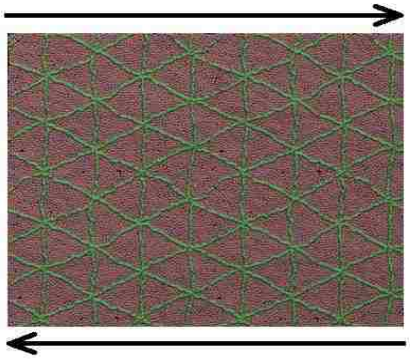

Figure 3.8 (a) RBC`s motion in shear flow proposed by Keller and Skalak (KS) model. (b) Initial condition of the Patch of Erythrocyte Membrane at the High-Stress Region.

To simulate this phenomenon in LAMMPS with the LJ model, we need to transfer pN force to the LJ unit system force scale. For LJ style, all physical quantities have no unit. We first need to determine three main parameters (σ, τ, and ε) to define the pN force, and the method of determination is described in LAMMPS documentation. The parameters to be used are the following:

$$\boldsymbol{\sigma} = 5 \text{ nm}$$

$$\boldsymbol{\tau} = 0.1 \text{ μs}$$

$$\boldsymbol{\varepsilon} = 0.269 \text{ kcal/mol}$$

These parameters are taken from Fu et al. [12]. Using these, we calculated the shear force to be applied on our coarse-grained patch to determine pore formation under different shear force values. To do that, we first need to convert pN forces into LJ units.

From the LAMMPS documentation: force = epsilon/sigma, where f* = f sigma / epsilon.

After inserting values, we have: $F = F^{*} \times 35.7 * 10^{-12}$ Newton.

Table 3.1 Shear forces and their converted values to LAMMPS units [16].

	F = 5 pN	F = 10 pN	F = 15 pN	F = 20 pN	F = 25 pN	F = 50 pN
$F^{*} = F/ 35.7$	0.140056	0.28011204	0.42016806	0.56022409	0.70028011	1.40056022

Shear forces are applied symmetrically to the patch region through to the opposite sides, as shown in **figure 3.5 (B).** Shear-induced pore formation is observed on the highest stress region. We applied several forces starting from 5 pN to 25 pN by increasing 5 pN at each stage. We summed up all pore areas that are drawn with yellow circles to create the entire pore formation area that are illustrated as black circles. In addition to that, we considered

pore size as two times greater than size of the bead. Total patch area is 14400 nm^2 . Entire process are shown by taken snapshots as follows:

(A)

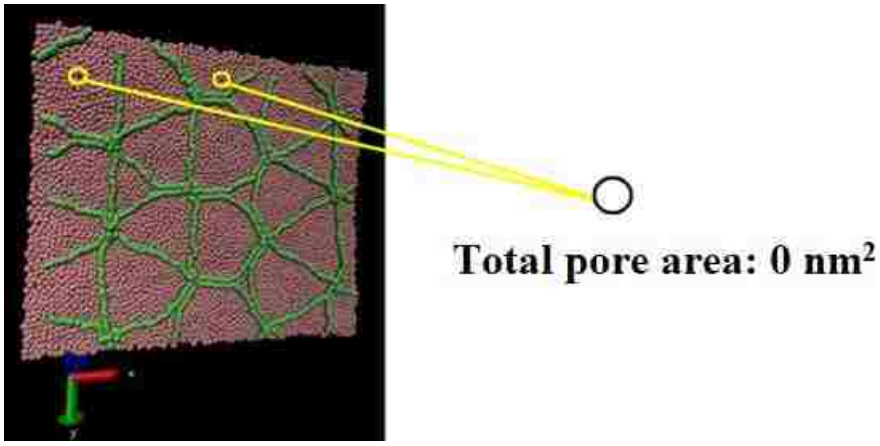

(B)

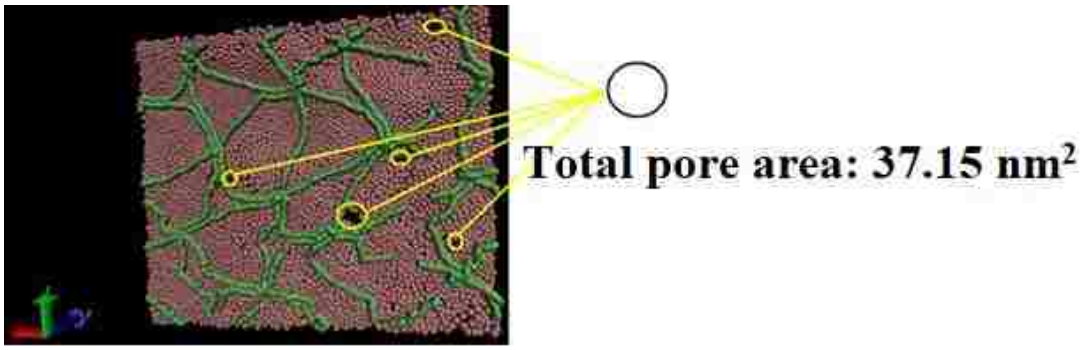

(C)

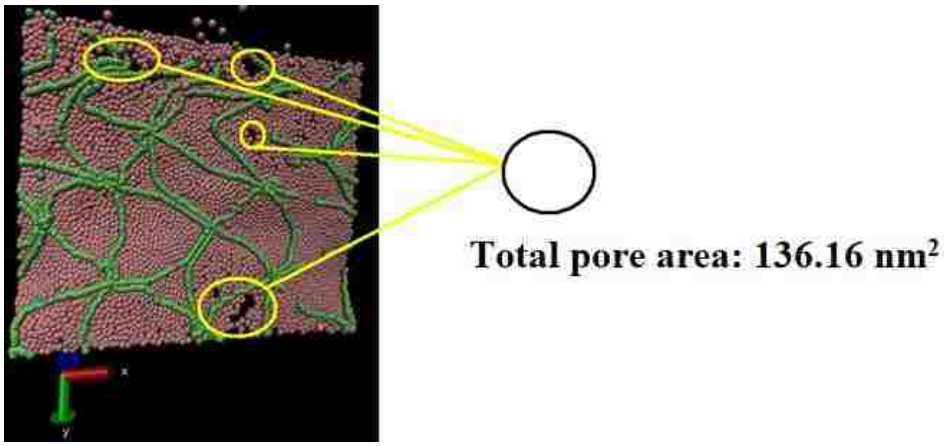

(D)

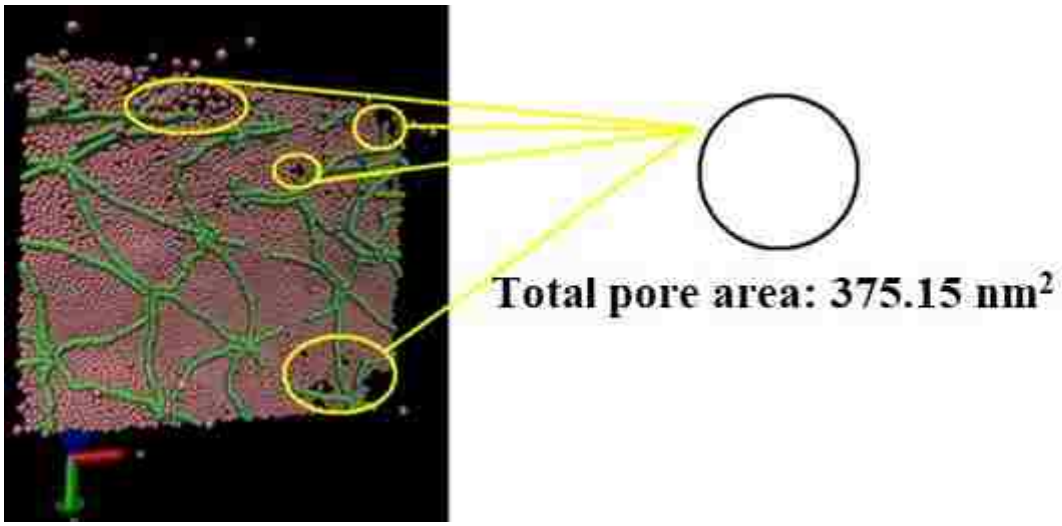

(E)

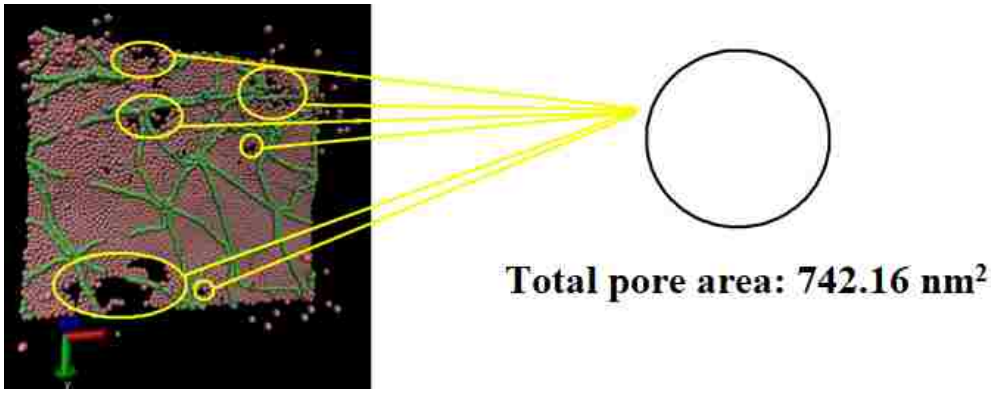

Figure 3.9 Shear–induced pore formations on the high stress/strain region of the patch of coarse–grained cytoskeletal is given as snapshots in here. The shear forces applied to the patch as were follows: (A) = 5pN, (B) = 10pN, (C) = 15pN, (D) = 20pN, (E) = 25pN [17].

(A)

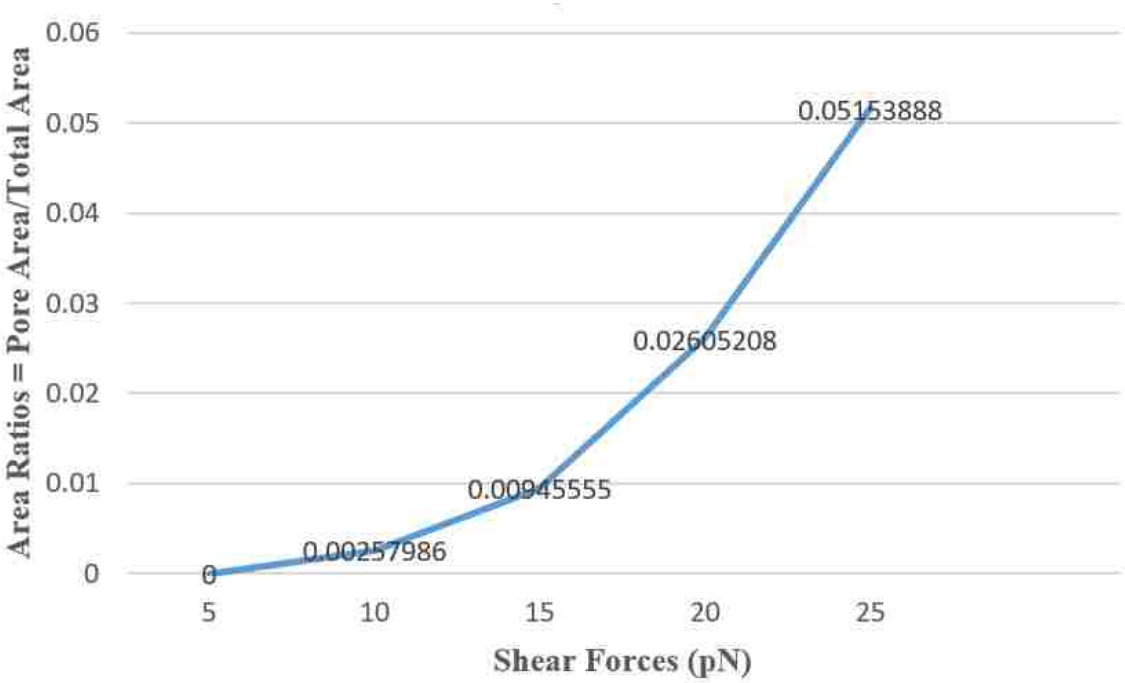

Figure 3.10 (a) Shear (pN) forces versus the area ratios at the high-stress region.

3.4 – Conclusion and Future Work

Conclusion

Mechanical response of the patch of human erythrocyte has been studied in coarse – grained scale using molecular dynamic methods with interest on membrane diffusion and diffusivity, membrane tension, rupture, and shear-induced pore area.

First, we validated the patch of erythrocyte membrane by modeling diffusivity and determining the diffusion coefficient constant. We recognized that beads behave like a fluid structure as results of linearly increasing the diffusivity.

Second, we stretched the patch of the coarse-grained erythrocyte membrane uniformly until rupture. The critical stress/strain from simulation match with those obtained in experiments in laser optical tweezers trapping a bead. Then, we defined surface tension, both circular tether membrane and our modelled patch, to compare the surface tension to our modelled patch, which was ten times bigger than that obtained experiment's surface tension.

Lastly, we determined the pore area of the patch of erythrocyte membrane at the high-stress region over a range of deformations. We observed that lipid membrane’s beads rupture from the membrane on the highest stress regions and this rearing significantly increase when we increase force at each stage.

Future Work

In our future model, first, we will investigate how the diffusivity and diffusion coefficients can be changed under a variety of surface tensions. Those coefficient parameters can be used on the SN model for the purpose of capturing singular phenomena at molecular level.

Second, we count on the effects of membrane curvature on our coarse-grained model to further investigate how it may affect our obtained results.

Lastly, we will link CGMD to the mesoscale spring model with a finite element method by defining the required parameters.

REFERENCE

1. Mary Louise Turgeon (2004). Clinical Hematology: Theory and Procedures. Lippincott Williams & Wilkins. p. 100. ISBN 9780781750073.

   Retrieved from

   https://trove.nla.gov.au/work/8892155

2. Mclaren, E., & Brittenham, M. (2018). Statistical and graphical evaluation of erythrocyte volume distributions. American Journal of Physiology Heart and Circular Physiology, 252(4)(10).

   Retrieved from

   https://doi.org/10.1152/ajpheart.1987.252.4.H857

3. Bianconi, E., Piovesan, A., Facchin, F., Beraudi, A., Frabetti, F., Vitale, L., … Canaider, S. (2013). Annals of Human Biology An estimation of the number of cells in the human body, 4460.

   Retrieved from

   https://doi.org/10.3109/03014460.2013.807878

4. SEER Training Modules, U. S. National Institutes of Health, National Cancer Institute. (2018, October 18) Classification & Structure of Blood Vessels.

   Retrieved from

   https://training.seer.cancer.gov/anatomy/cardiovascular/blood/classification.html

5. Richard Skalak, P. I. B. (1969). Deformation of Red Blood Cells in Capillaries. Science (SCIENCE), 164(3880)(C), 717–719.

   Retrieved from

   http://science.sciencemag.org/content/164/3880/717

6. Shu, Chien A. Luse, Sarah A. Bryant, C. (1971). Hemolysis during filtration through micropores: a scanning electron microscopic and hemorheological correlation. Microvascular Research, 203, 183–203.
Retrieved from
https://www.ncbi.nlm.nih.gov/pubmed/4938960

7. Kmiecik, Sebastian; Gront, Dominik; Kolinski, Michal; Wieteska, Lukasz; Dawid, Aleksandra Elzbieta; Kolinski, Andrzej (2016-06-22). "Coarse-Grained Protein Models and Their Applications". Chemical Reviews. 116: 7898–936.
Retrieved from
https://pubs.acs.org/doi/10.1021/acs.chemrev.6b00163

8. Introduction to Molecular Dynamics Simulation Using LAMMPS (2017). Faculty of Science, Univ. of Manitoba, Winnipeg Compute Canada / West Grid.
Retrieved from
https://www.westgrid.ca/files/Intro_MD_Simulations_LAMMPS_0.pdf

9. Potentials Energy Functions (2018). Professor A. Martini, Purdue University.
Retrieved from
https://nanohub.org/resources/7574/download/Martini_L2_PotentialEnergyFunctions.pdf

10. Li, J., Lykotrafitis, G., Dao, M., & Suresh, S. (2007). Cytoskeletal dynamics of human erythrocyte. Proceedings of the National Academy of Sciences, 104(12), 4937–4942.
Retrieved from
https://doi.org/10.1073/pnas.0700257104

11. Li, H., & Lykotrafitis, G. (2012). Two-Component Coarse-Grained Molecular-Dynamics Model for the Human Erythrocyte Membrane, 102(January). Retrieved from https://doi.org/10.1016/j.bpj.2011.11.4012

12. Fu, S. P., Peng, Z., Yuan, H., Kfoury, R., & Young, Y. N. (2017). Lennard-Jones type pair-potential method for coarse-grained lipid bilayer membrane simulations in LAMMPS. Computer Physics Communications, 210(October), 193–203. Retrieved from https://doi.org/10.1016/j.cpc.2016.09.018

13. Blood Flow in Capillaries (2018) Retrieved from http://www.bg.ic.ac.uk/research/k.parker/homepage/Mechanics%20of%20the%20Circulation/Chap_13/_Chapter_13b.htm

14. Auth, T., & Gov, N. S. (2009). Diffusion in a fluid membrane with a flexible cortical cytoskeleton. *Biophysical Journal*, *96*(3), 818–830. Retrieved from https://doi.org/10.1016/j.bpj.2008.10.038

15. Paul, R., Tasnim, T., Dhar, R., Mojumder, S., Saha, S., & Motalab, M. A. (2017). Study of Uniaxial Tensile Properties of Hexagonal Boron Nitride Nanoribbons. ArXiv, 7–12. Retrieved from https://doi.org/10.1109/TENCON.2017.8228335

16. Yunus, D. E., He, R., Shi, W., Kaya, O., & Liu, Y. (2017). Short fiber reinforced 3d printed ceramic composite with shear-induced alignment. Ceramics International, 43(15).

Retrieved from

https://doi.org/10.1016/j.ceramint.2017.06.012

17. Raucher, D., & Sheetz, M. ~P. (1999). Characteristics of a membrane reservoir buffering membrane tension, 77(4), 1992–2002.

Retrieved from

https://www.ncbi.nlm.nih.gov/pmc/articles/PMC1300480/

18. Dupire, J., Abkarian, M., & Viallat, A. (2015). A simple model to understand the effect of membrane shear elasticity and stress-free shape on the motion of red blood cells in shear flow. Soft Matter, 11(42), 8372–8382.

Retrieved from

https://doi.org/10.1039/c5sm01407g

19. R Nave (2018) Surface Tension

Retrieved from

http://hyperphysics.phy-astr.gsu.edu/hbase/surten2.html

VITA

Orhan Kaya was born to Yazgül Kaya and Hıdır Kaya on June 4th, 1988, in Istanbul, Turkey. He attended Inonu University and obtained his Bachelor of Science degree in Mechanical Engineering in 2012. After that he worked several jobs as a mechanical engineer. He then joined Dr. Yaling Liu's group at Lehigh University to pursue his master's degree in the department of mechanical engineering and mechanics.

EDUCATION

BSc. 2007 - 2012: Department of Mechanical Engineering, Inonu University

BSc. 2010 - 2011: Department of Mechanical Engineering, Yildiz Technical University (FARABI Scholarship & Exchange Program)

MSc. 2015 - 2016: Computational Science and Engineering, Istanbul Technical University (After being accepted to Lehigh University, he left Istanbul Technical University in 2016 without receiving any degree)

MSc. 2017-- 2019: Department of Mechanical Engineering & Mechanics, Lehigh University

PROFESSIONAL EXPERIENCE

HVAC AND PIPELINE ENGINEER **[08.10.2012 – 09.11.2013]**

ÇETİN MÜHENDİSLİK LTD. COMPANY ISTANBUL / TURKEY

JOB DESCRIPTION:

- I designed air heating, water heating, ventilation, and air conditioning systems compatible with all types of buildings and following the construction process to be done. Also, I designed different kinds of gas units for IGDAS. (Istanbul Gas Distribution Industry and Trade Incorporated Company)
- I used REVIT-MEP, AutoCAD, and GASLINE 3D Design and Analysis Programs.

FIELD SERVICE ENGINEER (Military Service) **[11.06.2013 – 05.04.2014]**

GENDARMERIE MAINTENANCE COMMAND AGRI / TURKEY

JOB DESCRIPTION:

- I served in the army for around six months. I was a control engineer at Maintenance Command, which handles the repair, overhaul and maintenance of all Otokar Akrep, Otokar Cobra, Dragoon 300, Cadillac V150/S, Shortland S55, and equipment. After working there for a few months, I transferred to the service department. (In Turkey, military service is compulsory for all male citizens. That is the custom here; I do not know if this is acceptable as a job or not.)

FOREIGN TRADE SPECIALIST **[06.11.2014 – 07.05.2014]**

PETES MACHINE INDUSTRY CORPORATE ISTANBUL / TURKEY

JOB DESCRIPTION:

- I was managing the process of the import and export of various lift tables, jacks, compressors, oiling equipment, lifts, garage equipment, and engineering parts between the company and partners.

OPERATING SYSTEM PROJECT **[09.10.2014 – 11/15/2015]**

C AND SYSTEM PROGRAMMERS ASSOCIATION ISTANBUL / TURKEY

JOB DESCRIPTION:

First, I took some courses as follows: C, C++, Unix/Linux System Programming and Assembly Language. Then, I accepted the operating system project on 08/15/2015. Our team's tasks were implementing low-level programs.

- To introduce the project, CSD is a new operating system being developed by C and System Programmers Association (CSD in Turkish, giving a name to the operating system). It has a graphical user interface and supports multithreaded preemptive operations on multicore hardware. The kernel is completely original; it is designed and implemented by the CSD members and is not a Linux derivative.

JOURNAL PAPER

D.Yunus, R. He, W. Shi, **O. Kaya**, Y. Liu, “Short Fiber Reinforced 3D Printed Ceramic Composite with Shear-Induced Alignment”, Ceramics International, in press, 2017